the total uterus tissues of the three groups of mice by bisulfite sequencing (Fig. 2A–C). There were 15 CpG sites spanning −272 to +199 of the promoter and the 5′-UTR (exon 1) region of SF-1. The percentages of total methylated CpG sites in this region, in control, and low and high-dose GEN, were 78.3%, 73.9%, and 54.4%, respectively, indicating that GEN dose-dependently induced demethylation in this region. Most CpG sites in the 5′-UTR (exon1) were demethylated by high-dose GEN. In particular, the methylation levels of 5 CpG sites between +45 and +89 were significantly lower in high-dose GEN than in control (Fisher's exact test, $P < 0.01$). We further split the endometrium to separate the luminal side (LU) from the basilar myometrial side (MY), and both specimens were separately subjected to bisulfite sequencing. This procedure was applied to the samples from the GEN-treated groups but not to control samples due to uterus atrophy. In low-dose GEN treated mice, the mean methylation levels of LU and MY were 84.8% and 65.0%, respectively (not shown). In high-dose GEN treated mice, the mean methylation levels of LU and MY were 42.1% and 66.7%, respectively (Fig. 2D). Thus, the demethylation induced by high-dose GEN occurred predominantly in the LU, rather than in the MY.

3.2. Effect of genistein on primary endometrial cell culture

In order to study the SF-1 promoter methylation at the cellular level, we employed an endometrial cell primary culture. Intact murine endometrium were divided into LU and MY portions, and cells were separately isolated. Primary cell clones were established by colony-formation, following the plating of a serially-titrated cell suspension (see Section 2). Efficient isolated colony formation was achieved with cells seeded at a density of 4,500–15,300 cells/cm^2. For LU and MY, the average frequencies of colony appearance were 7.5 per 10^5 cells and 15 per 10^5 cells, respectively. The growth curves of representative clones derived from LU and MY are shown in Fig. 3. Cell clones with highest and lowest proliferative activities were obtained from LU and MY, separately. More highly proliferative cells were obtained from MY than from LU (Fig. 3A and C). We selected 20 highly proliferative clones for further study (see Section 2). Two rapid growing clones obtained from MY showed self-renewal activity when secondarily seeded at a very low cell density (10 cells/cm^2) (not shown). To screen for primary cultured cells that responded to GEN, we set up a high-resolution melting (HRM) assay that identified region-specific methylation levels. The region analyzed by HRM assay exclusively contained the 7 CpG sites between +19 and +89 bp that were most differentially demethylated following oral administration of GEN (Fig. 2). Each clone was treated with or without GEN for 1 week; cells treated with a similar concentration of DMSO served as control. Among the 20 clones that we screened, only one GEN-treated clone (No. 16) exhibited a significant shift in the melting curve compared to control cells (Fig. 4A). This clone had the highest proliferation

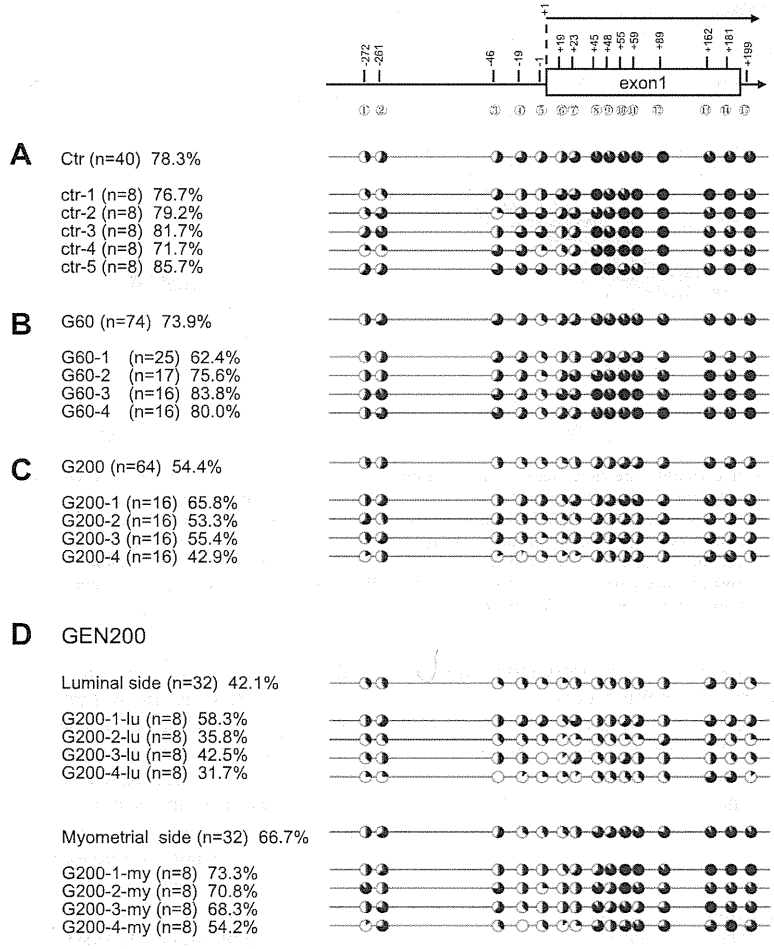

Fig. 2. Genistein induced demethylation of the SF-1 gene promoter in endometrial tissues of OVX mice. The schematic diagram indicates CpG locations on the SF-1 promoter region, spanning 5′-flanking to exon 1. The CpG position relative to the first base of exon 1 (+1) is shown. The bisulfite sequencing fragment contains 15 CpG sites. The black inlay represents the mean methylation levels of each CpG, and the left panel contains the number of sequenced clones and the mean methylation level of all CpGs. Summarized methylation results are shown at the top. (A–C) Difference in methylation levels between (A) vehicle (control), (B) low-dose GEN (60 mg/kg/d), and (C) high-dose GEN (200 mg/kg/d) exposed uteri. (D) Difference in methylation levels between luminal and myometrial sides of a uterus exposed to high-dose GEN.

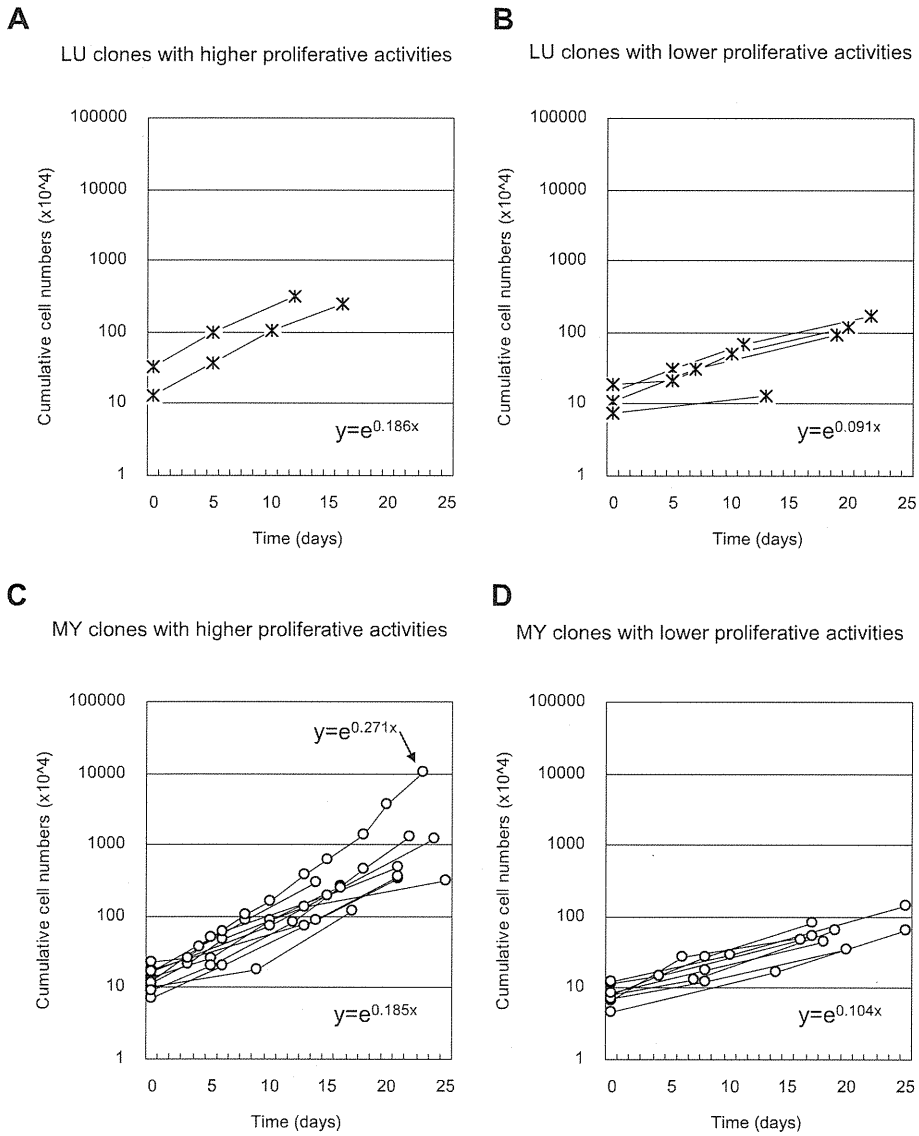

Fig. 3. Proliferation properties of isolated clones: one clone showed highly proliferative activity. Representative growth curves of clones harvested from intact murine endometrium are shown. Formula indicates the slope of fitted growth curves. Clones were divided into two groups: high and low proliferative (see Section 2). A total of 20 highly proliferative clones were analyzed by HRM after *in vitro* GEN treatment. (A, B) Asterisks indicate representative growth curves of cell clones isolated from luminal side. (A) Clones with higher proliferative activities, derived from luminal side. Six highly proliferative clones were obtained in total; 2 representatives are shown. (B) Clones with lower proliferative activities, derived from luminal side. (C, D) Each circle indicates representative growth curves of cell clones isolated from myometrial side. (C) Clones with higher proliferative activities, derived from the myometrial side. In total, 14 highly proliferative clones were obtained; 10 representatives are shown. The arrow indicates the clone with the most rapid growth. (D) Clones with lower proliferative activities, derived from myometrial side.

activity (Fig. 3C, arrow). GEN treatment of the other clones did not result in significant changes to the melting curve patterns (not shown). We further confirmed the methylation status of clone No. 16 by bisulfite sequencing. The percentages of CpG methylation in the SF-1-272 to +199 promoter regions for untreated and GEN-treated cells were 85.0% and 65.8%, respectively (Fig. 4B).

4. Discussion

Growing evidence suggests that the manner in which nutrients can either help maintain health, or conversely, promote disease development may be mediated by epigenetic regulation [12,20]. However, relatively little is known about tissue-specific sensitivity or how much plasticity exists in regards to the effect that a given environmental factor can exert on a certain epigenetic target [20,21]. GEN, a non-nutrient dietary component of soy products, exhibits mixed estrogen agonist and antagonist properties, and multiple functions both *in vivo* and *in vitro* [7,22]. Several animal studies have demonstrated that GEN acts as an epigenetic modulator [20]. We focused on the effects of GEN on endometrium, because endometrium is not only hormone responsive, but also a highly proliferative organ. Epigenetic alterations of proliferative tissue or cells may then be expanded through tissue proliferation. We used OVX rodents, which are a widely used model for studying estrogen withdrawal and replacement [23], as well as for the assessment of endocrine-disrupting chemicals in the environment [4]. In our experiment, GEN induced proliferation of the endometrium and increased uterine weight (Fig. 1A) to extents similar to those previously reported in OVX rats [4]. Our findings also suggested that GEN treatment induced marked demethylation of

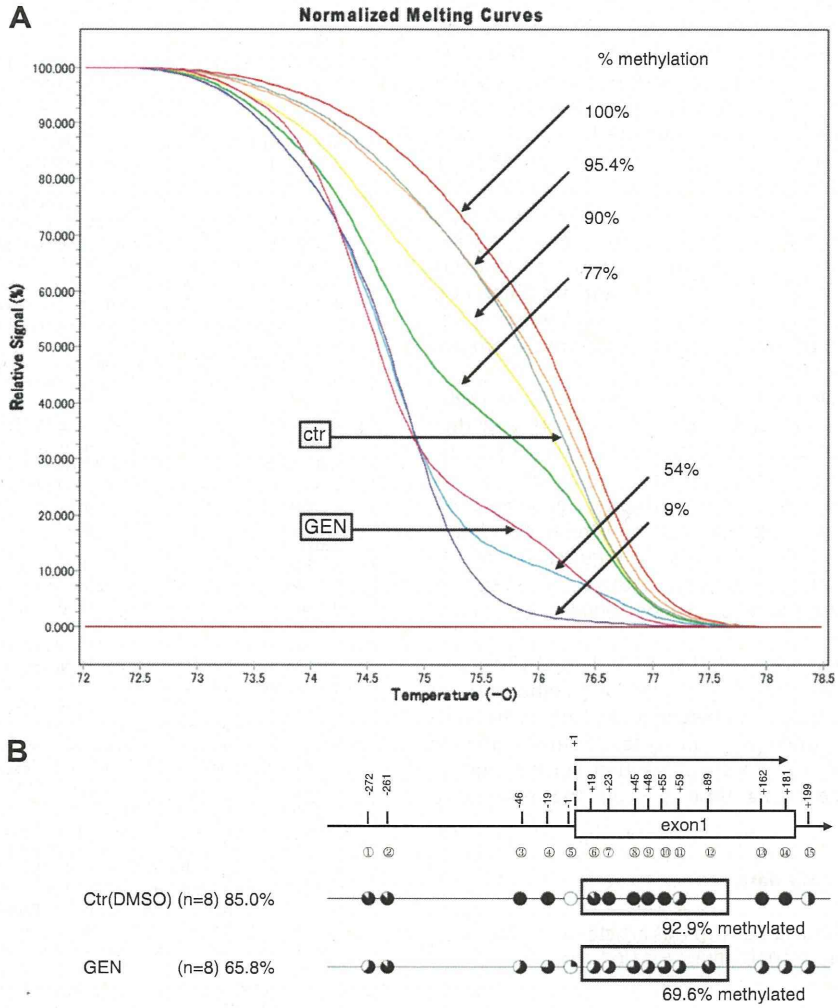

Fig. 4. Genistein induced demethylation of the SF-1 gene in the cell clone that showed the highest proliferative activity. (A) The GEN-mediated demethylation of CpGs (at the positions of +19, 23, 45, 48, 55, 59, and 89) in the SF-1 gene *in vitro* in one out of 20 isolated clones (Fig. 3A and C). HRM analysis enabled to clear separation of the PCR product mixtures with different CpG compositions. The methylation standards were prepared as 100% (red), 95.4% (orange), 90% (yellow), 77% (green), 54% (blue), and 9% (violet) methylated template in demethylated background. Grey and pink indicate the control and GEN-treated clone sample, respectively. (B) SF-1 DNA methylation status, obtained from bisulfate sequencing, of the clone that showed demethylation in HRM assay. Percentage under box (HRM region) indicates percent methylation of HRM region. (For interpretation of the references to color in this figure legend, the reader is referred to the web version of this paper.)

CpG sites in the SF-1 promoter (Fig. 2), and substantial increase in SF-1 mRNA level (Fig. 1B). Expressions of genes downstream of transcription factor SF-1 were also significantly enhanced (Fig. 1C–F). However, it should be noted that the induced mRNA levels were still very low (Fig. 1B–F), less than one copy per cell, as determined by the Percellome method [16]. Our results are consistent with those of a previous study reporting that a physiological concentration of GEN increased Cyp19a1 enzymatic activity in endometrial cells derived from a normal uterus, whereas GEN did not affect Cyp19a1 activity in a cell-free assay [24]. It is unknown whether GEN stimulated Cyp19a1 activity by epigenetic modulation.

In the present study, we also identified primary cultured endometrial cells that were competent for epigenetic regulation by GEN, which were present at a very low frequency. In our *in vitro* study, GEN treatment did not enhance, but rather inhibited the proliferation of colony-derived cells. Taken together, these findings indicate that a minor population of endometrium cells can respond to GEN and that, in these cells, GEN induces demethylation and activation of SF-1, followed by the induction of the SF-1 steroidogenic cascade. This might lead to local steroidogenesis and enhanced endometrium proliferation *in vivo* in GEN-treated OVX mice. Since demethylation of the SF-1 promoter was observed at the whole tissue level (Fig. 2), and the induced expression of steroidogenic genes occurred only to a subcellular amount (Fig. 1B–F), the demethylation event in each cell may not be sufficient for the SF-1 induction.

The demethylation in the endometrium that occurred after 1 week of treatment with high-dose GEN was more prominent in the LU than in the MY. Following GEN treatment, the methylation level in the MY was similar to that in the untreated endometrium as a whole. After 7 days of GEN exposure, the endometrial cells in the LU of OVX mice were composed of regenerated cells moving from MY to LU; in light of this, our results indicate that the initial epigenetic alteration might be expanded through proliferation of regenerating cells. This is also consistent with our observation that more endometrial cells derived from MY showed higher colony-formation activity and rapid proliferation than did those derived

from LU (Fig. 3). We thus speculate that there are GEN-sensitive cells in the MY, which might contain endometrial stem cells [25].

Recently, human endometrial stem cells were identified; they reside in endometrial stromal tissue and possess fibroblastic-shape and self-renewal ability, thus forming large, densely packed, homogenous colonies [17,18]. Some candidates for murine endometrial progenitor cells have been suggested to reside in the luminal epithelial or area of adjacent to the myometrium [25]. The rapidly growing endometrial cell that we obtained had a fibroblastic-shape, formed large, relatively homogenous, densely packed colonies, and showed self-renewal activity when seeded at a very low cell density (data not shown). Although there are differences between the species, we speculate that our rapid growing cell clones may correspond to the human endometrial stromal progenitors cells [17].

Aberrant SF-1 expression with lack of promoter CpG methylation has been reported in ectopic endometriosis [14], and thus endometriosis is now considered an epigenetic disease [26]. Endometriosis is classically defined as the growth of endometrial tissue at extrauterine sites; it has been suggested that each endometriotic lesion originates from a single epigenetically deregulated endometrial progenitor cell [27]. Further studies are required to identify cells which are competent for epigenetic changes following GEN exposure, and to elucidate the relationships between these cells, GEN, and endometriosis.

In conclusion, we demonstrated that GEN demethylates the promoter region of the SF-1 gene. This is the first demonstration of phytoestrogen participation in epigenetic alterations in adult endometrial tissue. These findings are important from standpoints of nutrition, public health, and disease prevention. Further study is warranted to characterize the nature of the cells that respond to GEN in the endometrium.

Appendix A. Supplementary data

Supplementary data associated with this article can be found, in the online version, at doi:10.1016/j.bbrc.2011.07.104.

References

[1] H. Adlercreutz, Phyto-oestrogens and cancer, Lancet Oncol. 3 (2002) 364–373.
[2] M. Messina, W. McCaskill-Stevens, J.W. Lampe, Addressing the soy and breast cancer relationship: review, commentary, and workshop proceedings, J. Natl. Cancer Inst. 98 (2006) 1275–1284.
[3] A.H. Wu, R.G. Ziegler, A.M. Nomura, D.W. West, L.N. Kolonel, P.L. Horn-Ross, R.N. Hoover, M.C. Pike, Soy intake and risk of breast cancer in Asians and Asian Americans, Am. J. Clin. Nutr. 68 (1998) 1437S–1443S.
[4] J. Kanno, L. Onyon, S. Peddada, J. Ashby, E. Jacob, W. Owens, The OECD program to validate the rat uterotrophic bioassay. Phase 2: dose–response studies, Environ. Health Perspect. 111 (2003) 1530–1549.
[5] K. Pettersson, J.A. Gustafsson, Role of estrogen receptor beta in estrogen action, Annu. Rev. Physiol. 63 (2001) 165–192.
[6] P. Diel, T. Hertrampf, J. Seibel, U. Laudenbach-Leschowsky, S. Kolba, G. Vollmer, Combinatorial effects of the phytoestrogen genistein and of estradiol in uterus and liver of female Wistar rats, J. Steroid Biochem. Mol. Biol. 102 (2006) 60–70.
[7] V. Beck, U. Rohr, A. Jungbauer, Phytoestrogens derived from red clover: an alternative to estrogen replacement therapy?, J Steroid Biochem. Mol. Biol. 94 (2005) 499–518.
[8] N. Sato, N. Yamakawa, M. Masuda, K. Sudo, I. Hatada, M. Muramatsu, Genome-wide DNA methylation analysis reveals phytoestrogen modification of promoter methylation patterns during embryonic stem cell differentiation, PLoS One 6 (2011) e19278.
[9] S.M. Meeran, A. Ahmed, T.O. Tollefsbol, Epigenetic targets of bioactive dietary components for cancer prevention and therapy, Clin. Epigenetics 1 (2010) 101–116.
[10] S. Majid, A.A. Dar, V. Shahryari, H. Hirata, A. Ahmad, S. Saini, Y. Tanaka, A.V. Dahiya, R. Dahiya, Genistein reverses hypermethylation and induces active histone modifications in tumor suppressor gene B-Cell translocation gene 3 in prostate cancer, Cancer 116 (2010) 66–76.
[11] A.K. Jha, M. Nikbakht, G. Parashar, A. Shrivastava, N. Capalash, J. Kaur, Reversal of hypermethylation and reactivation of the RARbeta2 gene by natural compounds in cervical cancer cell lines, Folia. Biol. (Praha) 56 (2010) 195–200.
[12] Y. Li, T.O. Tollefsbol, Impact on DNA methylation in cancer prevention and therapy by bioactive dietary components, Curr. Med. Chem. 17 (2010) 2141–2151.
[13] K. Morohashi, S. Honda, Y. Inomata, H. Handa, T. Omura, A common trans-acting factor, Ad4-binding protein, to the promoters of steroidogenic P-450s, J. Biol. Chem. 267 (1992) 17913–17919.
[14] Q. Xue, Z. Lin, P. Yin, M.P. Milad, Y.H. Cheng, E. Confino, S. Reierstad, S.E. Bulun, Transcriptional activation of steroidogenic factor-1 by hypomethylation of the 5′ CpG island in endometriosis, J. Clin. Endocrinol. Metab. 92 (2007) 3261–3267.
[15] S.E. Bulun, H. Utsunomiya, Z. Lin, P. Yin, Y.H. Cheng, M.E. Pavone, H. Tokunaga, E. Trukhacheva, E. Attar, B. Gurates, M.P. Milad, E. Confino, E. Su, S. Reierstad, Q. Xue, Steroidogenic factor-1 and endometriosis, Mol. Cell. Endocrinol. 300 (2009) 104–108.
[16] J. Kanno, K. Aisaki, K. Igarashi, N. Nakatsu, A. Ono, Y. Kodama, T. Nagao, "Per cell" normalization method for mRNA measurement by quantitative PCR and microarrays, BMC Genomics 7 (2006) 64.
[17] R.W. Chan, K.E. Schwab, C.E. Gargett, Clonogenicity of human endometrial epithelial and stromal cells, Biol. Reprod. 70 (2004) 1738–1750.
[18] C.E. Gargett, K.E. Schwab, R.M. Zillwood, H.P. Nguyen, D. Wu, Isolation and culture of epithelial progenitors and mesenchymal stem cells from human endometrium, Biol. Reprod. 80 (2009) 1136–1145.
[19] Y. Kumaki, M. Oda, M. Okano, QUMA: quantification tool for methylation analysis, Nucleic Acids Res. 36 (2008) W170–W175.
[20] J.A. McKay, J.C. Mathers, Diet induced epigenetic changes and their implications for health, Acta Physiol. (Oxf) (2011) 103–118.
[21] B.C. Christensen, E.A. Houseman, C.J. Marsit, S. Zheng, M.R. Wrensch, J.L. Wiemels, H.H. Nelson, M.R. Karagas, J.F. Padbury, R. Bueno, D.J. Sugarbaker, R.F. Yeh, J.K. Wiencke, K.T. Kelsey, Aging and environmental exposures alter tissue-specific DNA methylation dependent upon CpG island context, PLoS Genet. 5 (2009) e1000602.
[22] C.B. Klein, A.A. King, Genistein genotoxicity: critical considerations of in vitro exposure dose, Toxicol. Appl. Pharmacol. 224 (2007) 1–11.
[23] G. Rimoldi, J. Christoffel, D. Seidlova-Wuttke, H. Jarry, W. Wuttke, Effects of chronic genistein treatment in mammary gland, uterus, and vagina, Environ. Health Perspect. 115 (Suppl. 1) (2007) 62–68.
[24] K.M. Edmunds, A.C. Holloway, D.J. Crankshaw, S.K. Agarwal, W.G. Foster, The effects of dietary phytoestrogens on aromatase activity in human endometrial stromal cells, Reprod. Nutr. Dev. 45 (2005) 709–720.
[25] C.E. Gargett, H. Masuda, Adult stem cells in the endometrium, Mol. Hum. Reprod. 16 (2010) 818–834.
[26] S.W. Guo, Epigenetics of endometriosis, Mol. Hum. Reprod. 15 (2009) 587–607.
[27] Y. Wu, Z. Basir, A. Kajdacsy-Balla, E. Strawn, V. Macias, K. Montgomery, S.W. Guo, Resolution of clonal origins for endometriotic lesions using laser capture microdissection and the human androgen receptor (HUMARA) assay, Fertil. Steril. 79 (Suppl. 1) (2003) 710–717.

nature cell biology

PKA-dependent regulation of the histone lysine demethylase complex PHF2–ARID5B

Atsushi Baba[1], Fumiaki Ohtake[1,2], Yosuke Okuno[1,2], Kenichi Yokota[1], Maiko Okada[1,2], Yuuki Imai[1,3], Min Ni[3], Clifford A. Meyer[4], Katsuhide Igarashi[5], Jun Kanno[5], Myles Brown[3] and Shigeaki Kato[1,2,6]

Reversible histone methylation and demethylation are highly regulated processes that are crucial for chromatin reorganization and regulation of gene transcription in response to extracellular conditions. However, the mechanisms that regulate histone-modifying enzymes are largely unknown. Here, we characterized a protein kinase A (PKA)-dependent histone lysine demethylase complex, PHF2–ARID5B. PHF2, a jmjC demethylase, is enzymatically inactive by itself, but becomes an active H3K9Me2 demethylase through PKA-mediated phosphorylation. We found that phosphorylated PHF2 then associates with ARID5B, a DNA-binding protein, and induce demethylation of methylated ARID5B. This modification leads to targeting of the PHF2–ARID5B complex to its target promoters, where it removes the repressive H3K9Me2 mark. These findings suggest that the PHF2–ARID5B complex is a signal-sensing modulator of histone methylation and gene transcription, in which phosphorylation of PHF2 enables subsequent formation of a competent and specific histone demethylase complex.

Post-translational modifications of histone amino-terminal tails, including reversible acetylation, methylation, phosphorylation and ubiquitylation, modulate both chromatin structure and gene regulation[1,2]. Reversible histone methylation defines the state of chromatin; repressive histone methylation marks such as H3K9Me2 inhibit gene transcription from nearby promoters, and removal of these marks by histone lysine demethylases permit transcription. Thus, enzymes such as jmjC (Jumonji C)-domain-containing histone lysine demethylases seem to play pivotal roles in epigenetic control[3–10]. Though histone marks are altered in response to extracellular signals, the underlying mechanism by which this is achieved is largely unknown.

RESULTS

Identification of the PHF2–ARID5B histone H3K9Me2 demethylase complex

During biochemical identification of transcriptional co-regulators for nuclear receptors[11,12], we purified a number of direct interactants for nuclear receptors. Among them, a co-activator complex for FXR (farnesoid X receptor) from HepG2 cells was selected for further analysis, because its abundance in the purified fractions was significantly increased when the cells were pretreated with forskolin (FSK), a protein kinase A (PKA) activator (Supplementary Fig. S1a). Matrix-assisted laser desorption/ionization–time of flight mass spectrometry analysis of the purified complex[11,12] identified three subunits: plant homeodomain (PHD) finger two (PHF2; ref. 13), AT-rich interactive domain 5B (ARID5B) isoform α and ARID5B isoform β (ref. 14; Fig. 1a and Supplementary Fig. S1b–e). The complex was still detectable after further column purification (Supplementary Fig. S1f). ARID5B contains the ARID/Bright domain, which is seen in subunits of chromatin-remodelling complexes and is considered to be a sequence-specific/nonspecific DNA-attachment domain[14]. PHF2 (ref. 13) contains PHD and jmjC domains[4,6]. Unlike several other jmjC histone demethylases[3,5,8,9], PHF2 lacks the ARID domain. PHF2 and ARID5B genes are expressed in a broad range of tissues, including liver (Supplementary Fig. S2c), and at protein levels as well in various cell lines (Supplementary Fig. S2a,b,d). PHF2 physically interacted with FXR and HNF4α (hepatocyte nuclear factor 4α; Supplementary Fig. S3a,b,d), but not with ERα (oestrogen receptor alpha) or VDR (vitamin D receptor; Supplementary Fig. S3c,d). PHF2 directly interacted with ARID5B *in vitro* (Supplementary Fig. S3e–g).

The PHF2–ARID5B complex was purified from HepG2 cells stably expressing Flag–PHF2. As jmjC-domain-containing proteins catalyse lysine demethylation[3–10], we investigated the histone lysine demethylation activity of the purified PHF2 complex[7,10]. The PHF2 complex exhibited lysine demethylase activity *in vitro* as assessed by a formaldehyde release (Fig. 1b). Then we examined

[1]Institute of Molecular and Cellular Biosciences, University of Tokyo, 1-1-1 Yayoi, Bunkyo-ku, Tokyo 113-0032, Japan. [2]ERATO, Japan Science and Technology Agency, 4-1-8 Honcho, Kawaguchishi, Saitama 332-0012, Japan. [3]Department of Medical Oncology, Dana-Farber Cancer Institute and Harvard Medical School, Boston, Massachusetts 02115, USA. [4]Department of Biostatistics and Computational Biology, Dana-Farber Cancer Institute and Harvard School of Public Health, Boston, Massachusetts 02115, USA. [5]Division of Cellular and Molecular Toxicology, National Institute of Health Sciences, 1-18-1 Kamiyoga, Setagaya-ku, Tokyo 158-8501, Japan.
[6]Correspondence should be addressed to S.K. (e-mail: uskato@mail.ecc.u-tokyo.ac.jp)

Received 14 July 2011; accepted 28 February 2011; published online 1 May 2011; DOI: 10.1038/ncb2228

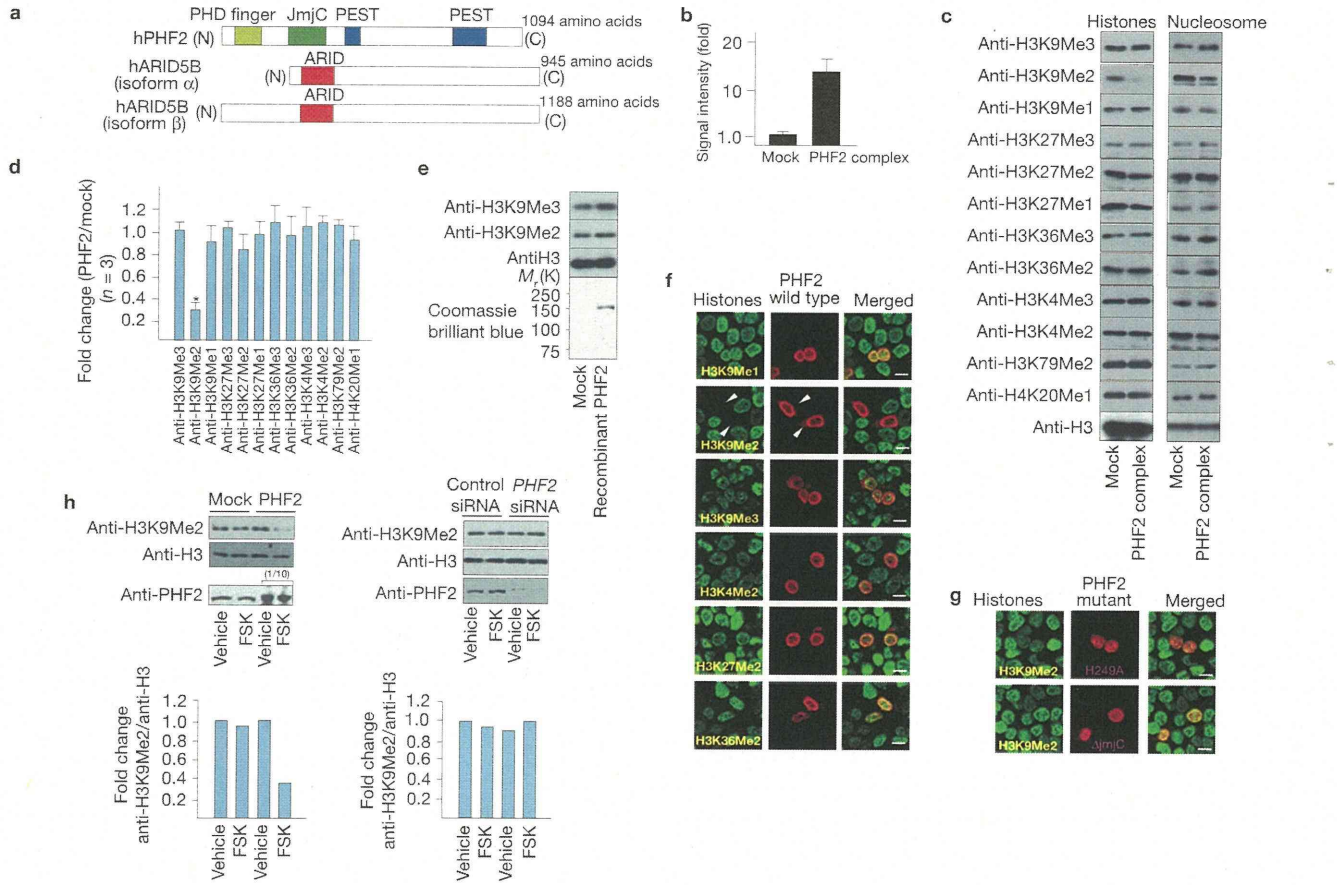

Figure 1 Identification of the PHF2–ARID5B histone H3K9Me2 demethylase complex. (**a**) A schematic representation of domains of PHF2 and ARID5B. (**b–d**) Histone H3K9Me2 demethylase activity of the purified PHF2 complex *in vitro*. (**b**) Native histones were incubated with PHF2 complex, and formaldehyde release was analysed by fluorescence detection. Shown is the average ± s.d. ($n = 3$) of the relative activity. (**c**) The PHF2 complex was incubated with purified native histones (left) or mononucleosomes (right) for demethylation reaction, and each modification was determined by western blotting as indicated. (**d**) Intensity of histone marks in the demethylation assay of native histones by PHF2 (in **c** and Supplementary Fig. S8a) was quantified, and averages ± s.d. of three independent experiments are shown. The asterisk shows $P < 0.05$ in Student's *t*-test. (**e**) Recombinant PHF2 protein is catalytically inactive. Recombinant PHF2 protein (lower panel) was subjected to *in vitro* demethylation assay (upper panels). (**f**) 293F cells were transfected with Flag–PHF2 expression vectors for 24 h and treated with FSK for 6 h, then cells were fixed and immunostained with the indicated antibodies. Note the decreased level of H3K9Me2 in the anti-Flag-positive cells (arrowheads). Scale bars, 40 μm. (**g**) 293F cells were transfected with either the Flag–PHF2$^{\Delta jmjC}$ or the HA–PHF2^{H249A} mutant, and immunostaining was carried out as in **f**. Scale bars, 40 μm. (**h**) H3K9Me2 demethylation activity of PHF2 *in vivo*. 293F cells transfected with the indicated expression vectors or short interfering RNAs (siRNAs), and were treated with FSK for 6 h. The soluble chromatin fraction was subjected to western blotting as indicated. Uncropped images of blots are shown in Supplementary Fig. S9.

the site-specificity of lysine demethylation using native histones or purified mononucleosomes as substrates. *In vitro*, the PHF2 complex demethylated dimethylated Lys 9 on histone H3 (H3K9Me2), but neither mono- nor trimethylated H3K9 (H3K9Me1, Me3) (Fig. 1c,d). Methylated H3K4, K27, K36 and K79 and H4K20 seemed unlikely PHF2 substrates (Fig. 1c,d). Thus it is likely that PHF2 substrate recognition is more specific than the closely related PHF subfamily members such as PHF8 and KDM7/KIAA1718 (refs 15–17). This demethylase activity was not detected in recombinant PHF2 protein (Fig. 1e). PHF2 did not demethylate a methylated peptide (amino acids 1–21 of H3) containing K9Me2 (Supplementary Fig. S4a). Such substrate specificity is known for Lid2 (ref. 18) and yeast Lsd1 (ref. 19), and possibly due to requirement of other regions of H3. Immunostaining analysis of 293F cells confirmed that PHF2 almost entirely demethylated H3K9Me2 in the presence of FSK, but had only marginal effects on H3K27Me2 and the other tested methylated histones (Fig. 1f and Supplementary Fig. S4b). The conserved histidine residue within the PHF2 jmjC domain was required for enzymatic activity (Fig. 1g). In 293F cells, overexpression of PHF2 in the presence of FSK decreased H3K9Me2, whereas knockdown of PHF2 did not lead to global increase of this mark (Fig. 1h), raising the possibility that other H3K9 demethylase(s) may compensate for PHF2 in these cells.

PHF2 is phosphorylated by PKA at a specific serine residue

In a co-immunoprecipitation assay, association of PHF2 and ARID5B was inducible on FSK treatment of immortalized hepatocytes[20] both in the absence (Fig. 2a) and presence (Supplementary Fig. S4c) of a proteasomal inhibitor, MG132. Consistently, abundance of these proteins was not clearly affected by FSK treatment (Supplementary Fig. S4d). Therefore, we reasoned that phosphorylation of the factor(s) by PKA was a trigger to induce association. Endogenous PHF2, but not ARID5B, was phosphorylated by FSK treatment of the cells (Fig. 2b,c).

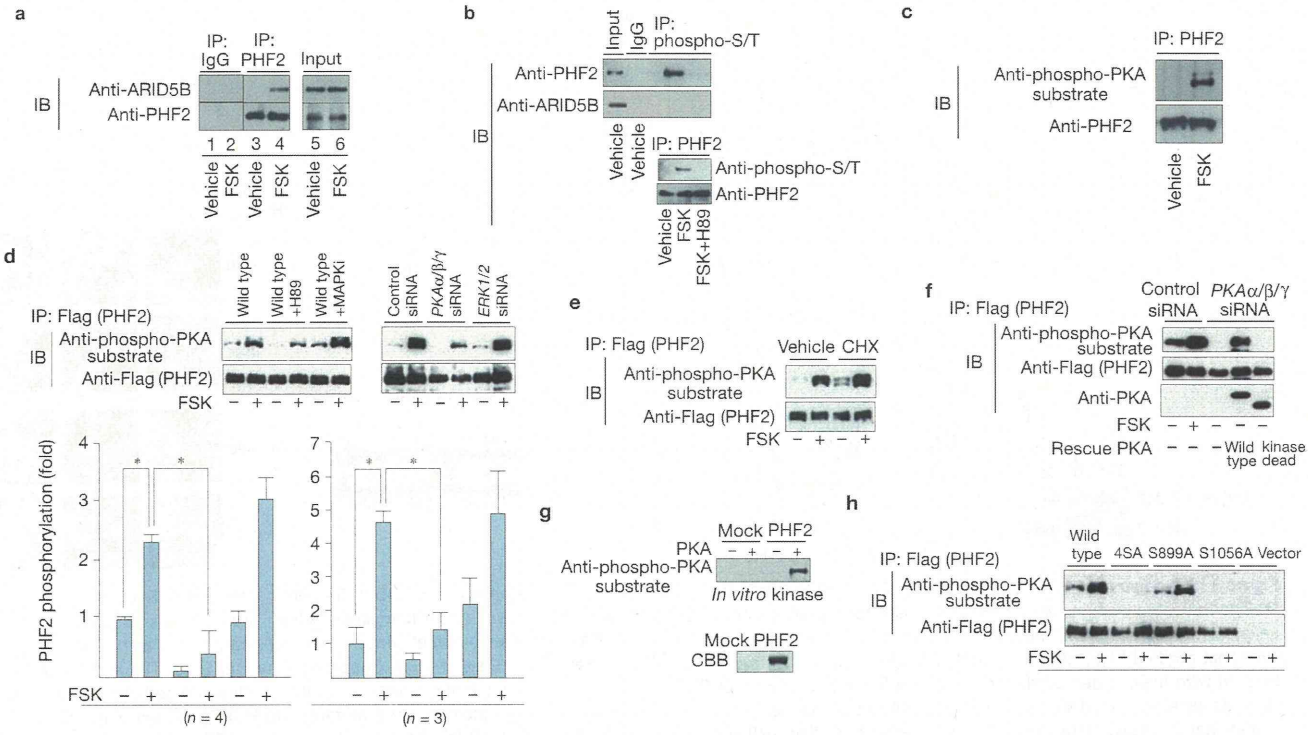

Figure 2 PKA-dependent complex assembly of PHF2–ARID5B. (**a**) Assembly of the endogenous PHF2–ARID5B complex. Hepatocytes were treated with the indicated compounds for 2 h and were subjected to immunoprecipitation (IP) and immunoblotting (IB) with the indicated antibodies. Specificity of antibodies was confirmed in Supplementary Fig. S2a,b. (**b**,**c**) Phosphorylation of endogenous PHF2 by PKA. Hepatocytes (**b**) or 293F cells (**c**) were treated with vehicle, FSK, or FSK +H89 as indicated for 2 h, then lysates were immunoprecipitated using either anti-phospho-serine/threonine or anti-PHF2 antibodies. The eluates were subjected to western blotting as indicated. (**d**–**f**) 293F cells transfected with Flag–PHF2 and indicated siRNAs were treated with the indicated inhibitors, and immunoprecipitated with anti-Flag antibodies. Immunoprecipitates were subjected to immunoblotting with an anti-phospho-PKA substrate antibody. (**d**, lower panel) Averages ± s.d. The other data sets are shown in Supplementary Fig. S8b,c. The asterisks show $P < 0.05$ in Student's *t*-test. (**g**) *In vitro* kinase assay with recombinant PHF2 and PKA proteins. (**h**) PHF2 is phosphorylated by PKA at Ser 757/899/954/1056. In the 4SA mutants, Ser 757/899/954/1056 were replaced with alanines. Uncropped images of blots are shown in Supplementary Fig. S9.

FSK-dependent PHF2 phosphorylation was negated by the PKA inhibitor H89, but not by a MAP kinase inhibitor (MAPKi; Fig. 2d). Cyclohexamide (CHX) did not attenuate PHF2 phosphorylation, indicating that this event does not mediate *de novo* protein synthesis (Fig. 2e). Knockdown of PKAα/β/γ, but not of extracellular signal-regulated kinases ERK1/2, abrogated PHF2 phosphorylation (Fig. 2d,f and Supplementary Fig. S5a). PKA phosphorylated recombinant PHF2 in *in vitro* phosphorylation assays (Fig. 2g). Using recombinant PHF2 deletion mutants, the carboxy-terminal region of PHF2 was mapped to be phosphorylated by PKA (Supplementary Fig. S5b,d), and bears four conserved, PKA consensus serine residues (Supplementary Fig. S5c). Replacement of all of four serine residues by alanines (4SA: Ser 757/Ser 899/Ser 954/Ser 1056) fully abrogated PKA phosphorylation of PHF2 (Fig. 2h). Further mapping revealed that Ser 1056 seemed to be a major phosphorylation site (Fig. 2h).

PKA-dependent demethylase activity of PHF2–ARID5B complex

We then asked if the demethylase activity of PHF2 for H3K9Me2 was also PKA dependent with proteins purified from 293F cells as well as recombinant proteins. Purified PHF2 protein, phosphorylated by PKA *in vitro*, exhibited H3K9Me2 demethylase activity (Fig. 3a–c). Conversely, PHF2 phosphorylated by FSK treatment in cells exhibited the demethylase activity, but *in vitro* dephosphorylation by BAP (bacterial alkaline phosphatase) negated the demethylase activity (Fig. 3b,c). ARID5B was dispensable for the enzymatic activity of PHF2 *in vitro* (Fig. 3b,c), because ARID5B was absent from the purified PHF2 protein fraction used (Supplementary Fig. S5f). Similarly, recombinant PHF2 was activated by PKA phosphorylation (Fig. 3d–f). PHF2 phosphorylation mutants were not activated by PKA (Fig. 3g). Consistent with the *in vitro* analyses, H3K9Me2 demethylation by overexpression of PHF2–ARID5B in cells was significantly enhanced by FSK treatment, but 4SA was not activated by FSK (Fig. 3h). Subnuclear localization patterns of the PHF2^{4SA} mutant did not look identical to that of wild-type PHF2 (Fig. 3h), raising the possibility that PHF2 phosphorylation is indispensable for chromatin association. Together, these findings suggest that PKA-mediated phosphorylation induces the demethylase activity of PHF2, unlike the other characterized jmjC demethylases exhibiting constitutive enzymatic activities both *in vivo* and *in vitro* as recombinant proteins[4–10].

ARID5B directs PKA-dependent promoter targeting of PHF2

We examined how PKA-mediated activation of the PHF2–ARID5B complex activated transcription at endogenous promoters. In immortalized hepatocytes, glucagon–PKA signalling regulates glucose

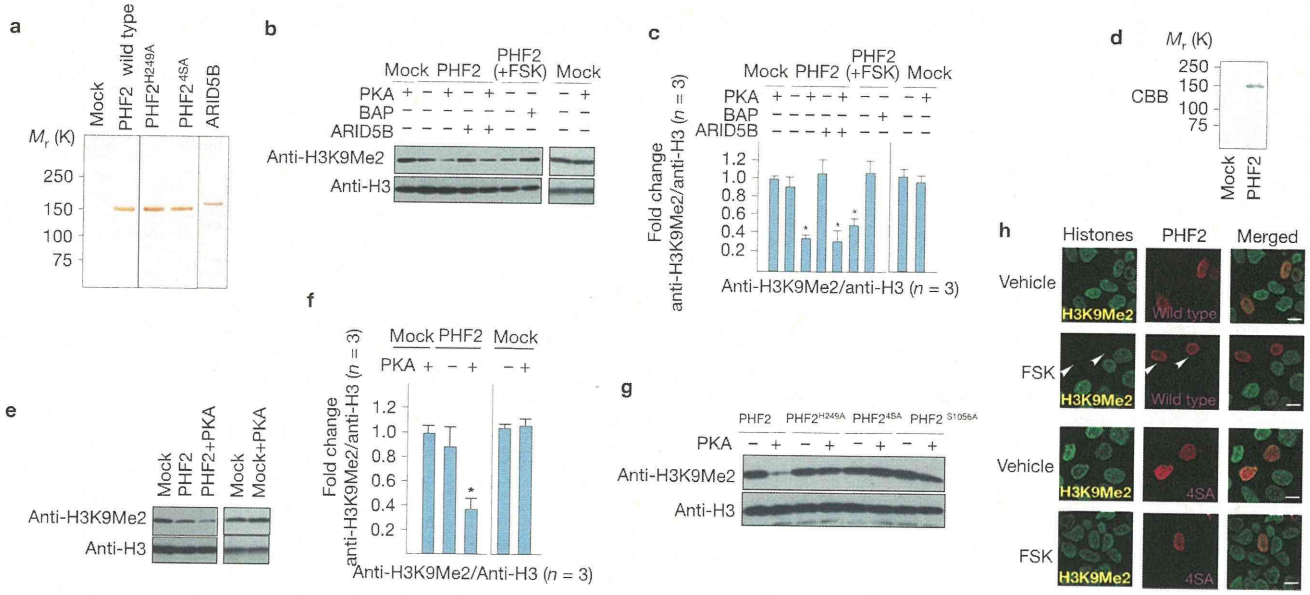

Figure 3 PKA-dependent demethylase activity of the PHF2–ARID5B complex. (**a**) The indicated proteins were purified to near homogeneity from 293F cells. Purification of PHF2 mutants is shown in Supplementary Fig. S5e. Note that purified PHF2 did not include ARID5B (Supplementary Fig. S5f). (**b**,**c**) *In vitro* histone demethylation assay. Purified PHF2 protein or PHF2 mutants were incubated with either PKA or BAP as indicated, and *in vitro* demethylation assays were carried out with/without purified ARID5B protein. (**c**) The signal intensity of three independent experiments (performed as in **b** and Supplementary Fig. S8d) was quantified. Data are averages ± s.d. The asterisks show $P < 0.05$ in Student's *t*-test. (**d**–**f**) Recombinant PHF2 protein purified to near homogeneity from Sf9 cells was phosphorylated by PKA, and *in vitro* demethylation assay was carried out as in **b**,**c**. (**f**) Data are averages ± s.d. ($n = 3$, Supplementary Fig. S8e). The asterisk shows $P < 0.05$ in Student's *t*-test. (**g**) *In vitro* histone demethylation assay as in **b** with the indicated PHF2 mutants. (**h**) H3K9Me2 demethylation activity of PHF2–ARID5B is FSK dependent *in vivo*. 293F cells transfected with wild-type or PHF2^{4SA} were treated with FSK for 6 h. Scale bars, 40 μm. Uncropped images of blots are shown in Supplementary Fig. S9.

homeostasis through induction of gluconeogenic enzymes, such as Pepck and G6Pase (refs 20–23). Chromatin immunoprecipitation (ChIP) analysis revealed glucagon–PKA-induced promoter binding of PHF2–ARID5B at the promoters of *Pepck* and *G6Pase* (Fig. 4a). Sequential ChIP (Re-ChIP) suggested that the endogenous PHF2–ARID5B complex associates with the *Pepck* promoter (Fig. 4b), without protein synthesis (Fig. 4b and Supplementary Fig. S6a). H89 abrogated glucagon-mediated recruitment of these factors (Supplementary Fig. S6b). PHF2 and ARID5B were co-recruited to *Pepck* promoter on similar time-courses (Supplementary Fig. S6c). Demethylation of H3K9Me2 was induced by FSK, coupled with PHF2 recruitment (Fig. 4a and Supplementary Fig. S6c). However, the H3K9Me1 level was not significantly altered by FSK treatment (Fig. 4a), suggesting that newly produced H3K9Me1 was sequentially demethylated by other H3K9 demethylase(s). H3K9Me3 signal was low in both the presence and absence of FSK (Fig. 4a), consistent with the notion that *Pepck* and *G6Pase* gene promoters are converted to euchromatin in hepatocytes.

We further explored the mechanism for PKA-dependent promoter recruitment of PHF2–ARID5B. Although ARID5B was dispensable for PHF2 enzymatic activity *in vitro* (Fig. 3b), ARID5B was required for promoter targeting of PHF2 and H3K9Me2 demethylation *in vivo* (Fig. 4c, lanes 9–12, 4d). Knockdown of PHF2 by RNA interference attenuated FSK-induced recruitment of ARID5B to the promoters (Fig. 4c, lanes 3–4, 4d), indicating the signal-sensing role of PHF2 in directing the complex to target promoters. A specific PHF2 mutant (H249A), lacking a conserved histidine essential for its lysine demethylation activity (Fig. 1g), was unable to anchor PHF2–ARID5B on the target gene promoter (Fig. 4c, lanes 7, 8). We reasoned that a lysine demethylation event occurred before chromatin association. Therefore, we determined whether ARID5B was a substrate for the PHF2 demethylase. Exogenously expressed ARID5B was lysine-methylated in hepatocytes in the absence of FSK (Fig. 5a, lane 2). PHF2 induced demethylation of ARID5B in the presence of FSK through the jmjC domain (Fig. 5a, lanes 3–4). ARID5B, but not other ARID family proteins, harbours a lysine motif (Lys 336) in the ARID domain that resembles the alignment around histone H3K9 (Supplementary Fig. S6d). When Lys 336 of ARID5B was replaced by alanine (K336A), the methylated form of ARID5B was no longer detected (Fig. 5a, lane 5). An anti-ARID5B-K336Me2 antibody was raised, and the specificity was confirmed by an enzyme-linked immunosorbent assay with methylated ARID5B (Supplementary Fig. S6e) as well as with unmethylated K336A or K336R mutants (Fig. 5b). We found that PHF2 promoted demethylation of ARID5B at Lys 336 (Fig. 5c). Catalytically inactive PHF2^{H249A} increased the ARID5B K336Me2 mark (Fig. 5c), and endogenous ARID5B was demethylated following FSK treatment (Fig. 5d). Moreover, purified PHF2 protein demethylated ARID5B at Lys 336 *in vitro* (Fig. 5e). We then used a DNA pulldown (ABCD) assay to determine if demethylation of Lys 336-methylated ARID5B converted it to an active form on DNA binding. Only when cells were treated with FSK, ARID5B–PHF2 complex was recruited to synthetic oligonucleotides containing the *Pepck* promoter sequences[24,25] (Fig. 5f). FSK-dependent DNA binding of PHF2–ARID5B was abolished in PHF2^{H249A} and ARID5B^{K336A} mutants (Fig. 5f). Neither PHF2^{H249A} nor ARID5B^{K336A} supported FSK-mediated promoter recruitment and subsequent H3K9Me2 demethylation (Fig. 4c).

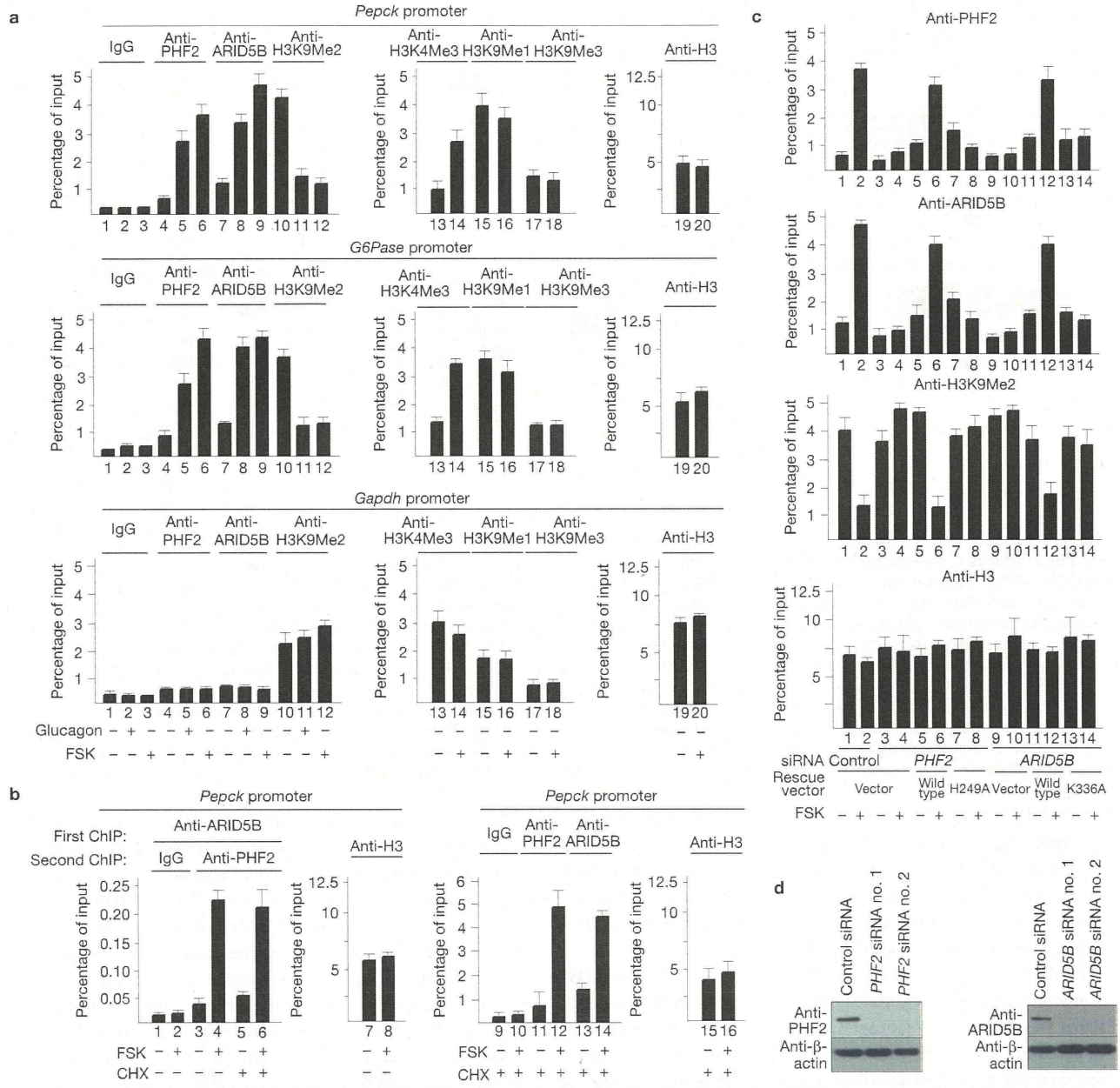

Figure 4 PKA-dependent promoter targeting of PHF2–ARID5B. (**a**) Endogenous PHF2–ARID5B complex is recruited to the promoter regions of *Pepck* and *G6Pase*, but not to that of *Gapdh*, in a glucagon–PKA-dependent manner. Hepatocytes were treated with the indicated compounds for 4 h, and ChIP assays were carried out using indicated antibodies. Data are average ± s.d. ($n = 3$). (**b**) ChIP and Re-ChIP assays. Hepatocytes were treated with the indicated compounds for 4 h, then sequentially immunoprecipitated with the indicated antibodies. Data are average ± s.d. ($n = 3$). (**c**) Promoter targeting and H3K9Me2 demethylase activities of PHF2–ARID5B mutants in ChIP assays. Hepatocytes were transfected with the indicated siRNAs for 24 h, then with the indicated rescue vector for a further 12 h. Then, cells were treated with FSK for 4 h and ChIP assays were carried out. Data are average ± s.d. ($n = 3$). (**d**) The knockdown efficiencies of siRNAs in immortalized hepatocytes were determined using samples in **c**. Uncropped images of blots are shown in Supplementary Fig. S9.

PHF2–ARID5B acts as a co-activator for HNF4α in liver of fasted mice

The transcriptional effects mediated by PHF2–ARID5B were assessed by monitoring gene expression in hepatocytes. PKA-dependent gene induction of *Pepck* and *G6Pase* was impaired (Fig. 6a) following knockdown of PHF2 or ARID5B in hepatocytes (Fig. 4d). The unphosphorylated PHF2 mutant ($PHF2^{4SA}$) was unable to confer the FSK response (Fig. 6a). As HNF4α is activated by the glucagon–PKA signalling pathway and serves as the primary transcriptional activator on *Pepck* and *G6Pase* promoters[21,22,26–28], we further characterized the transcriptional co-activation function of PHF2–ARID5B towards HNF4α. In a luciferase reporter assay in the presence of FSK (refs 12,29), PHF2 acted as a co-activator for HNF4α (Fig. 6b) as well as FXR (Supplementary Fig. S7) in 293F

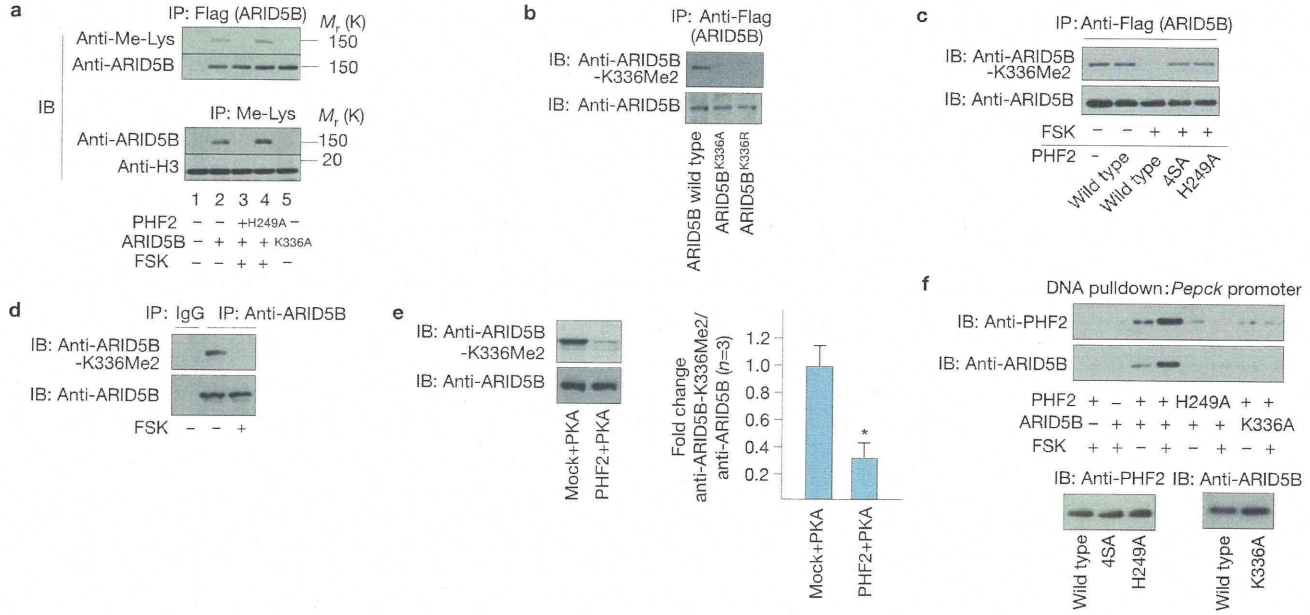

Figure 5 ARID5B directs PKA-dependent promoter targeting of PHF2. (**a**) PHF2 induces demethylation of ARID5B. The methylation state of ARID5B in 293F cells was examined using anti-ARID5B and anti-methyl-lysine antibodies. Wild-type, but not K336A, ARID5B is a lysine-methylated protein. (**b**) Confirmation of specificity of anti-ARID5B-K336Me2 antibody. 293F cells were transfected with the indicated ARID5B mutants and immunoprecipitated/blotted with the indicated antibodies. (**c**) Demethylation of ARID5B is dependent on the catalytic activity of PHF2 in hepatocytes as revealed by the specified anti-ARID5B-K336Me2 antibody. (**d**) Lys 336 methylation of endogenous ARID5B. 293F cells were treated with FSK for 4 h, then immunoprecipitation was carried out as indicated. (**e**) *In vitro* ARID5B demethylation assay. Flag–ARID5B purified from 293F cells was incubated with purified PHF2 (Fig. 3a), and the demethylation was detected by western blotting. The signal intensity of three independent experiments (in the upper panel and in Supplementary Fig. S8f) was quantified. Data are averages ± s.d. ($n = 3$). The asterisk shows $P < 0.05$ in Student's t-test. (**f**) DNA pulldown assay. The demethylase activity of PHF2 and the ARID domain of ARID5B are required for promoter DNA binding of PHF2–ARID5B in 293F cells. Cell lysates were mixed with avidin beads which were bound to biotin-conjugated oligonucleotides bearing the indicated promoter sequence. The bound protein was detected by western blotting. There were similar levels of expression of PHF2–ARID5B and their derivatives (lower panels). Uncropped images of blots are shown in Supplementary Fig. S9.

cells[24,25]. HNF4α was enriched with PHF2–ARID5B on the promoter of *Pepck* (Fig. 6c). Knockdown of HNF4α decreased recruitment of PHF2–ARID5B to the promoters (Fig. 6c) and loss of PKA-dependent gene induction (Fig. 6d). Thus, HNF4α and FXR have emerged as transcriptional activators co-activated by PHF2–ARID5B in glucagon–PKA-induced gene expression.

Finally, the physiological relevance of the proposed PHF2–ARID5B promoter targeting was examined under fasting conditions where PKA signal was activated by glucagon in intact animals. In fasted mice, co-recruitment of PHF2 with ARID5B was detected in the promoter regions of *Pepck* and *G6Pase* in liver (Fig. 6e) with the expected decrease in H3K9Me2 modification (Fig. 6e).

DISCUSSION

Here, we have identified a PKA-dependent histone demethylase complex that conferred signal-dependent activation of its responsive genes. Assembly of the PHF2–ARID5B complex, its recruitment to target promoters, and its H3H9Me2 demethylase activity were dependent on PKA activity. Thus, the PHF2–ARID5B complex seems to serve as a signal-sensing epigenetic determinant through removal of a repressive histone methylation mark[1,2,30,31] on the transcriptionally responsive promoters. The molecular basis of signal sensing by the PHF2–ARID5B complex is attributable to PKA-phosphorylation-dependent induction of PHF2 enzymatic activity and complex assembly with the DNA-binding subunit (ARID5B). Unlike PHF2, several other jmjC demethylases possess both jmjC and ARID domains within a single molecule[3,5,8,9]. Thus, segregation of these two key domains into separate subunits may enable PHF2 enzymatic activity to be linked to PKA signalling through assembly of the PHF2–ARID5B complex and intracomplex communication. Similarly, other jmjC demethylases that are inactive as single subunits may be functionally regulated through post-translational modifications and assembly with their complex partner components. The characterization of a signal-dependent histone demethylase provides further understanding of the regulatory mechanism for dynamic epigenetic modification in physiological contexts such as energy metabolism and homeostasis. □

METHODS

Methods and any associated references are available in the online version of the paper at http://www.nature.com/naturecellbiology

Note: Supplementary Information is available on the Nature Cell Biology website

ACKNOWLEDGEMENTS

We thank D. D. Moore for critical discussion, R. Sato and J. Inoue for providing materials, N. Moriyama and S. Fujiyama for technical assistance and M. Yamaki for manuscript preparation. This work was supported in part by Priority Areas from the Ministry of Education, Culture, Sports, Science and Technology, MEXT, Japan, JSPS, and The Naito Foundation (to F.O. and S.K.).

AUTHOR CONTRIBUTIONS

A.B., F.O. and S.K. designed the study. A.B., F.O., Y.O., K.Y., M.O. and Y.I. carried out experiments. M.N., C.A.M., K.I., J.K. and M.B. carried out analyses and provided general support. F.O. and S.K. wrote the paper.

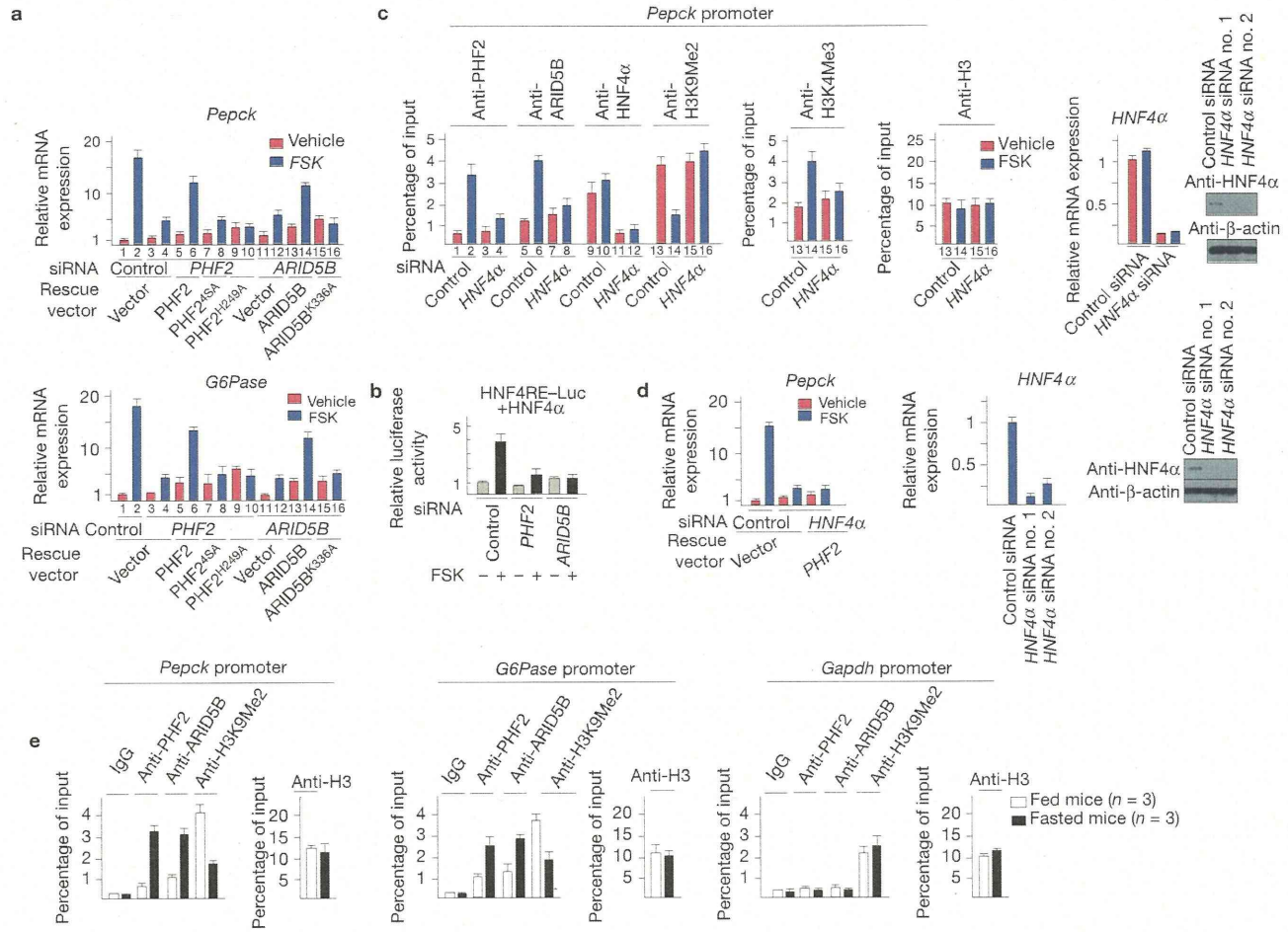

Figure 6 PHF2–ARID5B co-activates HNF4α in liver of fasted mice. (**a**) PHF2–ARID5B complex is indispensable for PKA-dependent gene induction of *Pepck* and *G6Pase*. Hepatocytes were transfected with the indicated siRNAs for 24 h, then incubated with the indicated compounds for 24 h, and quantatitive PCR with reverse transcription (RT–PCR) was carried out. Data are average ± s.d. ($n = 3$). (**b**) PHF2–ARID5B co-activates HNF4α in the presence of FSK in luciferase assays. 293F cells were transfected with the indicated plasmids in the presence or absence of FSK for 24 h. Data are average ± s.d. ($n = 3$). (**c**,**d**) Immortalized hepatocytes were transfected with HNF4α siRNA for 48 h, and ChIP assay (**c**) and quantitative RT–PCR for gene expression (**d**) were carried out. Knockdown efficiency was determined in the right panels of (**c**) and (**d**). Data are average ± s.d. ($n = 3$). (**e**) Livers from either fasted or fed mice ($n = 3$) were subjected to ChIP analyses using either anti-PHF2, anti-ARID5B, anti-H3K9Me2 or control IgG and anti-H3 antibodies. Fasting induces recruitment of PHF2–ARID5B and reduction of the H3K9Me2 mark in *Pepck* and *G6Pase* promoters, but not *Gapdh* promoter. Data shown are average ± s.d. of three independent experiments. Uncropped images of blots are shown in Supplementary Fig. S9.

COMPETING FINANCIAL INTERESTS
The authors declare no competing financial interests.

Published online at http://www.nature.com/naturecellbiology
Reprints and permissions information is available online at http://www.nature.com/reprints

1. * Kouzarides, T. Chromatin modifications and their function. *Cell* **128,** 693–705 (2007).
2. Ruthenburg, A. J., Li, H., Patel, D. J. & Allis, C. D. Multivalent engagement of chromatin modifications by linked binding modules. *Nat. Rev. Mol. Cell Biol.* **8,** 983–994 (2007).
3. Iwase, S. *et al.* The X-linked mental retardation gene SMCX/JARID1C defines a family of histone H3 lysine 4 demethylases. *Cell* **128,** 1077–1088 (2007).
4. Klose, R. J., Kallin, E. M. & Zhang, Y. JmjC-domain-containing proteins and histone demethylation. *Nat. Rev. Genet.* **7,** 715–727 (2006).
5. Lee, M. G., Norman, J., Shilatifard, A. & Shiekhattar, R. Physical and functional association of a trimethyl H3K4 demethylase and Ring6a/MBLR, a polycomb-like protein. *Cell* **128,** 877–887 (2007).
6. Shi, Y. & Whetstine, J. R. Dynamic regulation of histone lysine methylation by demethylases. *Mol. Cell* **25,** 1–14 (2007).
7. Tsukada, Y. *et al.* Histone demethylation by a family of JmjC domain-containing proteins. *Nature* **439,** 811–816 (2006).
8. Christensen, J. *et al.* RBP2 belongs to a family of demethylases, specific for tri- and dimethylated lysine 4 on histone 3. *Cell* **128,** 1063–1076 (2007).
9. Klose, R. J. *et al.* The retinoblastoma binding protein RBP2 is an H3K4 demethylase. *Cell* **128,** 889–900 (2007).
10. Whetstine, J. R. *et al.* Reversal of histone lysine trimethylation by the JMJD2 family of histone demethylases. *Cell* **125,** 467–481 (2006).
11. Ohtake, F. *et al.* Dioxin receptor is a ligand-dependent E3 ubiquitin ligase. *Nature* **446,** 562–566 (2007).
12. Takada, I. *et al.* A histone lysine methyltransferase activated by non-canonical Wnt signalling suppresses PPAR-gamma transactivation. *Nat. Cell Biol.* **9,** 1273–1285 (2007).
13. Hasenpusch-Theil, K. *et al.* PHF2, a novel PHD finger gene located on human chromosome 9q22. *Mamm. Genome* **10,** 294–298 (1999).
14. Whitson, R. H., Huang, T. & Itakura, K. The novel Mrf-2 DNA-binding domain recognizes a five-base core sequence through major and minor-groove contacts. *Biochem. Biophys. Res. Commun.* **258,** 326–331 (1999).
15. Qi, H. H. *et al.* Histone H4K20/H3K9 demethylase PHF8 regulates zebrafish brain and craniofacial development. *Nature* **466,** 503–507 (2010).
16. Liu, W. *et al.* PHF8 mediates histone H4 lysine 20 demethylation events involved in cell cycle progression. *Nature* **466,** 508–512 (2010).
17. Tsukada, Y., Ishitani, T. & Nakayama, K. I. KDM7 is a dual demethylase for histone H3 Lys 9 and Lys 27 and functions in brain development. *Genes Dev.* **24,** 432–437 (2010).
18. Li, F. *et al.* Lid2 is required for coordinating H3K4 and H3K9 methylation of heterochromatin and euchromatin. *Cell* **135,** 272–283 (2008).

19. Lan, F. *et al. S. pombe* LSD1 homologs regulate heterochromatin propagation and euchromatic gene transcription. *Mol. Cell* **26,** 89–101 (2007).
20. Jiang, G. & Zhang, B. B. Glucagon and regulation of glucose metabolism. *Am. J. Physiol. Endocrinol. Metab.* **284,** E671–E678 (2003).
21. Lin, J., Handschin, C. & Spiegelman, B. M. Metabolic control through the PGC-1 family of transcription coactivators. *Cell Metab.* **1,** 361–370 (2005).
22. Mayr, B. & Montminy, M. Transcriptional regulation by the phosphorylation-dependent factor CREB. *Nat. Rev. Mol. Cell Biol.* **2,** 599–609 (2001).
23. Feige, J.N. & Auwerx, J. Transcriptional coregulators in the control of energy homeostasis. *Trends Cell Biol.* **17,** 292–301 (2007).
24. Goodwin, B. *et al.* A regulatory cascade of the nuclear receptors FXR, SHP-1, and LRH-1 represses bile acid biosynthesis. *Mol. Cell* **6,** 517–526 (2000).
25. Lu, T. T. *et al.* Molecular basis for feedback regulation of bile acid synthesis by nuclear receptors. *Mol. Cell* **6,** 507–515 (2000).
26. Koo, S. H. *et al.* The CREB coactivator TORC2 is a key regulator of fasting glucose metabolism. *Nature* **437,** 1109–1111 (2005).
27. Rhee, J. *et al.* Regulation of hepatic fasting response by PPARgamma coactivator-1α (PGC-1): requirement for hepatocyte nuclear factor 4α in gluconeogenesis. *Proc. Natl Acad. Sci. USA* **100,** 4012–4017 (2003).
28. Yoon, J. C. *et al.* Control of hepatic gluconeogenesis through the transcriptional coactivator PGC-1. *Nature* **413,** 131–138 (2001).
29. Fujiki, R. *et al.* GlcNAcylation of a histone methyltransferase in retinoic-acid-induced granulopoiesis. *Nature* **459,** 455–459 (2009).
30. Metzger, E. *et al.* LSD1 demethylates repressive histone marks to promote androgen-receptor-dependent transcription. *Nature* **437,** 436–439 (2005).
31. Rosenfeld, M. G., Lunyak, V. V. & Glass, C. K. Sensors and signals: a coactivator/corepressor/epigenetic code for integrating signal-dependent programs of transcriptional response. *Genes Dev.* **20,** 1405–1428 (2006).

DOI: 10.1038/ncb2228

METHODS

Plasmids. Full-length complementary DNAs of human PHF2, ARID5B (full length, β isoform), HNF-4α and FXR were inserted into pcDNA3 vectors (Invitrogen; ref. 11). Deletion mutants of PHF2 (amino acids 1–229 fused to amino acids 367–1103 for $PHF2^{\Delta jmjC}$) and ARID5B (amino acids 1–318 fused to amino acids 423–1188 for $ARID5B^{\Delta ARID}$) were amplified by PCR and cloned into pcDNA3 or pGEX4T-1 (Amersham). Point mutants of PHF2 (S1056A point mutation, or S797A, S899A, S954A and S1056A for $PHF2^{4SA}$) and PHF2 jmjC-domain point mutants (H249A, Y321A and H338A) and ARID5B were generated by site-directed mutagenesis. HNF4RE-tk–luciferase reporter plasmids were generated by insertion of the promoter region of consensus HNF4RE into a pGL3 luciferase plasmid[32]. FXRE-tk–luciferase reporter plasmids were generated by insertion of the promoter region of human SHP (−572 to −3) containing FXRE into a pGL3 luciferase plasmid. Other plasmids have been described previously[11,12,32,33].

Biochemical purification and separation of FXR- or PHF2-associated complexes. The hepatic tumour-derived HepG2 cells were incubated for 4 h with either FSK (1 μM) and/or H89 (1 μM), and the nuclear extracts were prepared as previously described. For purification of the FXR-associating complex, the nuclear extracts were bound to glutathione *S*-transferase (GST)–FXR(D/E)–His (amino acids 193–477) columns[11,12,33]. The bound complexes were eluted with reduced glutathione (15 mM) in elution buffer. Glycerol density gradients were carried out as previously described[11,12,33]. The complex fraction was further loaded onto a diethylaminoethyl column (Whatman), and eluted with different concentrations of NaCl (150 mM–1 M). The purified proteins were silver-stained, and identified by matrix-assisted laser desorption/ionization–time of flight mass spectrometry (Bruker)[11,12,33]. For purification of PHF2-associating complex, the nuclear extracts were loaded onto M2 anti-Flag agarose gel (Sigma, A2220, 069K6018). After washing with binding buffer, the bound proteins were eluted by incubation with 1.0 ml of the Flag peptide ($[EYKEEEK]_2$, 0.2 mg ml^{-1}) (Sigma).

***In vitro* and *in vivo* lysine demethylation assay.** The *in vitro* histone demethylation assays were carried out as previously described[7,10].

For preparation of demethylases from mammalian cells, 293F cells were transfected with Flag–PHF2 plasmid using Lipofectamine 2000 (Invitrogen). After 36 h, the cells were lysed with TNE (20 mM Tris at pH 7.8, 150 mM NaCl, 0.5 mM EDTA, 1% NP40). For phosphorylation of PHF2 *in vivo*, cells were treated with FSK (10^{-6} M) 2 h before harvest, and NaF/Na_2VO_3 added to TNE. Cell lysates were subjected to immunoprecipitation using anti-Flag antibody-conjugated beads (Sigma, A2220, 069K6018). Beads were washed three times with high-salt TNE (20 mM Tris at pH 7.8, 450 mM NaCl, 0.5 mM EDTA, 1% NP40), and then three times with EDTA-free TNE. For phosphorylation of PHF2 *in vitro*, beads were mixed with 20 μl PKA buffer (0.1 μg PKA (Upstate), 20 mM Tris at pH 7.5, 10 mM $MgCl_2$, 100 μM ATP and incubated for 1 h at 37 °C. Then, beads were washed three times with demethylase stock buffer (20 mM Tris at pH 7.5, 150 mM KCl, 10% glycerol). The prepared PHF2 protein was used immediately for the demethylation reaction. Alternatively, the purified proteins were eluted with Flag elution buffer (200 mg ml^{-1} Flag peptide, 20 mM Tris at pH 7.5, 450 mM KCl, 10% glycerol).

For preparation of recombinant proteins, recombinant Flag–PHF2 was purified using Bac-to-Bac baculovirus expression systems (Invitrogen) according to the manufacturer's instructions. The purified Flag–PHF2 complex was prepared as described in the section on biochemical purification.

For demethylase reaction, 2 μg of PHF2 protein or 0.2 μg of PHF2 complex was mixed with substrates (calf thymus histone (10 μg) (Sigma, H9250), purified mononucleosome (10 μg), Flag–ARID5B protein purified from 293F cells (2 μg) or dimethyl H3 (Lys 9) peptide 1–21 (0.2 μg) (Upstate 12–430)) in the reaction buffer (final volume 20 μl) (20 mM Tris-HCl at pH 7.5, 150 mM KCl, 50 μM $Fe(NH_4)_2(SO_4)_2$–$6H_2O$, 1 mM α-ketoglutarate, 1 mM ascorbate, 20 μM $ZnCl_2$). The mixtures were incubated at 37 °C for 12 h, terminated by boiling for 5 min in SDS sample buffer[7,10]. The histone modification or methylation of ARID5B was detected by specific antibodies (see the antibody section). The signal intensity of western blots was quantified using Scion Image.

For histone demethylase assay detecting formaldehyde release, purified PHF2 complex (0.2 μg) was incubated with native histones (10 μg) for 30 min according to the manufacturer's protocol using DetectXTM (LUMINOS, K010-F1).

For *in vivo* histone demethylation assay, cells were first lysed in TNE, and the pellet fraction was resuspended in TNE and sonicated for 20 s (Tomy SEIKO) to obtain the chromatin fraction[3,9,10,34].

Antibodies, immunoprecipitation and western blotting. Anti-PHF2 and anti-ARID5B polyclonal antibodies were raised against PHF2 peptides (5′-ERSVDVTDVTKQKDC-3′, 5′-CKPKPVRDEYEYVSD-3′, 5′-CAYKSDDSSDE-GSLH-3′) and ARID5B peptides (5′-CDTPQGRNSDHGEDE-3′, 5′-CTDQGSNSEK-VAEEA-3′, 5′-CEQTSKYPSRDMYRE-3′), respectively, by Operon Biotechnology. Anti-ARID5B K336Me2 antibody was raised using the dimethylated peptide (MKER(KMe2)TPIER: ARID5B K336Me2), and purified over a peptide affinity column (MBL). The antibodies that bound to the non-methylated peptide (MKERKTPIER) were removed using an affinity column. The specificity of the antibody toward K336Me2 over K336Me0, Me1 and Me3 peptides was determined in Supplementary Fig. S20 using enzyme-linked immunosorbent assays (MBL).

For immunoprecipitation, cells were treated with FSK (1 μM) or glucagon (200 nM) for 2 h and cells were lysed in TNE. Cell lysates were incubated with the indicated antibodies listed in Supplementary Table S1. A full list of antibodies and the dilutions used is given in Supplementary Table S1.

Cell culture, transfection and luciferase assays. Mouse immortalized hepatocytes, TLR2 cells, were obtained from RIKEN (cell no. RCB0750; ref. 35). The immortalized hepatocytes were cultured at 33 °C in DMEM containing 2% fetal bovine serum, 10 μg ml^{-1} transferrin, 1 μg ml^{-1} insulin and 10 ng ml^{-1} epidermal growth factor, using collagen-coated dishes. Other cell lines are cultured in DMEM supplemented with 10% fetal bovine serum. Cells were treated with glucagon (200 nM), FSK (1 μM), H89 (1 μM), CHX (1 μM), GW4064 (1 μM), dexametasone (10 nM) or 25-OH cholesterol (10 μg ml^{-1}) either for 24 h (luciferase assays), for 6 h (*in vivo* demethylation assays) or for 2 h (immunoprecipitation).

For luciferase assays, cells at 40–50% confluence were transfected with the indicated plasmids (0.25 μg reporter plasmids, 0.1 μg HNF4α, 0.1 μg FXR, 0.05 μg of PHF2) using Lipofectamine reagent (Gibco BRL). Luciferase activity was determined with the luciferase assay system (Promega) as previously described[11,12,32,33].

ChIP experiments. ChIP assays were carried out essentially as previously described[11,12,33]. Hepatocytes were treated with glucagon (200 nM), FSK (1 μM) and/or H89 (1 μM) for 4 h or as indicated. Then, cells were subjected to ChIP experiment as described[11]. The precipitated DNA fragments were amplified by quantitative PCR (qPCR; TAKARA). For qPCR with reverse transcription, the specific primer sets were designed and provided by TAKARA. The primer sets are shown in Supplementary Table S1.

Fasting responses in mice. All mice were maintained according to the protocol approved by the Animal Care and Use Committee of the University of Tokyo.

For ChIP assays[11], eight-week-old C57BL/6 male mice were either deprived of food or fed for 6 h. Livers were isolated, minced and fixed in PBS containing 1% formaldehyde at 4 °C overnight. The cells were washed in PBS twice, then sonicated in PBS containing 0.2 mM EDTA and 1% Triton X-100. The cell lysates were subjected to ChIP assays as previously described[11].

RNA isolation and qPCR. Messenger RNA was isolated as previously reported[33]. For qPCR with reverse transcription, the specific primer sets were designed and provided by TAKARA. The primer sequences are shown in Supplementary Table S1, and the amount was normalized using glyceraldehyde-3-phosphate dehydrogenase.

RNA interference experiments. The siRNAs as shown in Supplementary Table S1, together with siCONTROL non-targeting siRNA no. 2 (catalogue no. D-001210-02-20), were synthesized by and obtained from Dharmacon/Thermo, and were transfected using Lipofectamine 2000 reagent (Invitrogen) as previously described[11]. The two siRNAs used for each experiment, and the results of target sequence no. 1 (for PHF2, ARID5B and HNF4α) are shown.

Immunostaining. Immunostaining was carried out essentially as previously described[36]. 293F cells were transfected with PHF2 or its derivatives, and 12 h after the transfection the cells were treated with FSK for 6 h, then fixed and subjected to immunostaining[36]. Antibodies used are described in the antibody section.

***In vitro* and *in vivo* kinase assays.** Recombinant GST–PHF2 deletion mutants expressed in *Escherichia coli* (1 μg), or Flag–PHF2 and its derivatives (1 μg) immunoprecipitated from 293F cells using anti-Flag antibody and eluted by Flag peptide, were incubated with PKA (Upstate; 2 ng) in reaction buffer (20 mM Tris-HCl at pH 7.5, 10 mM $MgCl_2$, $\gamma -^{32}$P ATP) in the presence or absence of PKA inhibitor (10 μM H89) for 15 min at 30 °C.

For detection of phosphorylated proteins in cells, hepatocytes were treated with the indicated ligands for 2 h, then subjected to phospho-protein purification using a PhosphoProtein Purification Kit (QIAGEN; ref. 12). Alternatively, cell lysates were immunoprecipitated using anti-PHF2 or anti-Flag as indicated, then western

blotted using anti-phospho-PKA-substrate antibody (Cell Signaling Technology, 100G7E, 9624S). For statistical analysis, the signal intensity of western blots was quantified using Scion Image, and the average ± s.d. of four independent experiments was shown with Student's *t*-test.

DNA precipitation assays. DNA precipitation assays were carried out essentially as described[33,37]. Human *Pck1* promoter (−312 ~ 23) was amplified by PCR using biotinylated primers. Then, the biotinylated DNA was annealed and bound to avidin beads (Invitrogen). 293F cells were transfected with Flag-ARID5B, HA-PHF2 and their derivatives, and incubated with/without FSK for 2 h. Cell lysates were incubated with the DNA-bound avidin beads for 30 min in TNE buffer. The samples were subjected to western blotting[33,37].

32. Unno, A. *et al.* TRRAP as a hepatic coactivator of LXR and FXR function. *Biochem. Biophys. Res. Commun.* **327,** 933–938 (2005).
33. Ohtake, F. *et al.* Modulation of oestrogen receptor signalling by association with the activated dioxin receptor. *Nature* **423,** 545–550 (2003).
34. Yokoyama, A., Takezawa, S., Schule, R., Kitagawa, H. & Kato, S. Transrepressive function of TLX requires the histone demethylase LSD1. *Mol. Cell Biol.* **28,** 3995–4003 (2008).
35. Puigserver, P. *et al.* Insulin-regulated hepatic gluconeogenesis through FOXO1-PGC-1α interaction. *Nature* **423,** 550–555 (2003).
36. Okada, M. *et al.* Switching of chromatin-remodelling complexes for oestrogen receptor-alpha. *EMBO Rep.* **9,** 563–568 (2008).
37. Fujiki, R. *et al.* Ligand-induced transrepression by VDR through association of WSTF with acetylated histones. *EMBO J.* **24,** 3881–3894 (2005).

nature cell biology

SUPPLEMENTARY INFORMATION

DOI: 10.1038/ncb2228

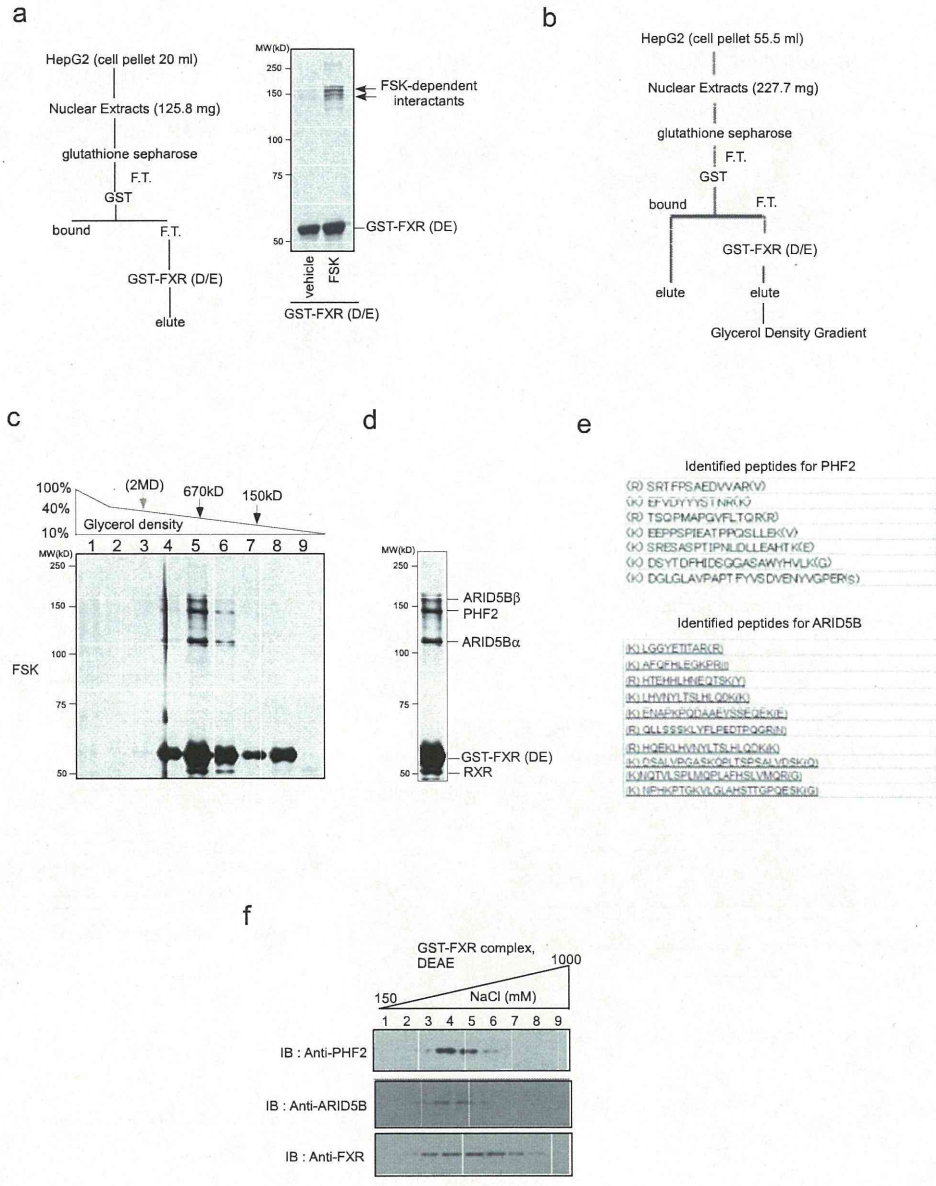

Figure S1 Purification of PHF2/ARID5B complex. **a,** Purification of a signal-dependent GST-FXR-associated proteins from HepG2 cells. Nuclear extracts from FSK-treated HepG2 cells were loaded on GST-FXR-bound glutathione sepharose beads. The bound proteins were analyzed by silver staining. **b,** The scheme for the purification of nuclear receptor-associating complexes. The experimental details were supplied in the supplemental methods. **c,** Purification of a GST-FXR-associated complex from HepG2 cells. Nuclear extracts from FSK-treated HepG2 cells were loaded on GST-FXR-bound glutathione sepharose beads. The eluted complexes were separated by glycerol density gradients as indicated. **d, e,** The isolated complexes were silver stained, and each protein was identified by MALDI-TOF/MS and fingerprinting. **f,** PHF2 and ARID5B form a complex with GST-FXR. The purified GST-FXR-associating complex in (c) was further separated by DEAE column with different NaCl concentrations. The elutants were subjected to Western blotting.

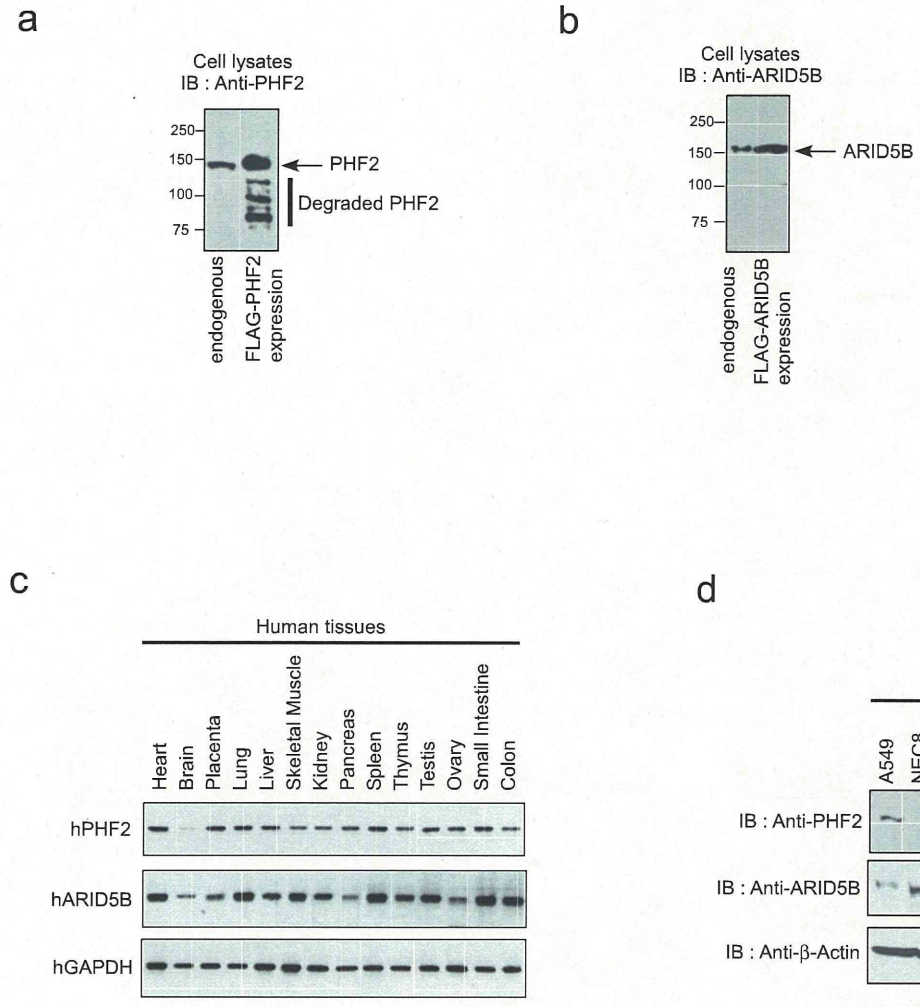

Figure S2 The expression profiles of PHF2 and ARID5B. **a, b,** Specificity confirmation of the newly raised antibodies. Normal 293F cell lysates or lysates transfected with the indicated expression vectors were subjected to Western blotting. This confirmed that these anti-PHF2 (a) and anti-ARID5B (b) antibodies detect endogenous proteins with high specificity. **c**, The mRNA expression profiles of human PHF2 and ARID5B. The mRNA levels of PHF2 and ARID5B were determined by semi-quantitative PCR using cDNAs from human tissues (Clontech, human cDNA panel, #636742 and #636743). **d**, Protein expression of PHF2 and ARID5B in various human cell lines. Total cell lysates were prepared from the indicated human cell lines. Equal amounts of proteins were subjected to Western blotting with the indicated antibodies.

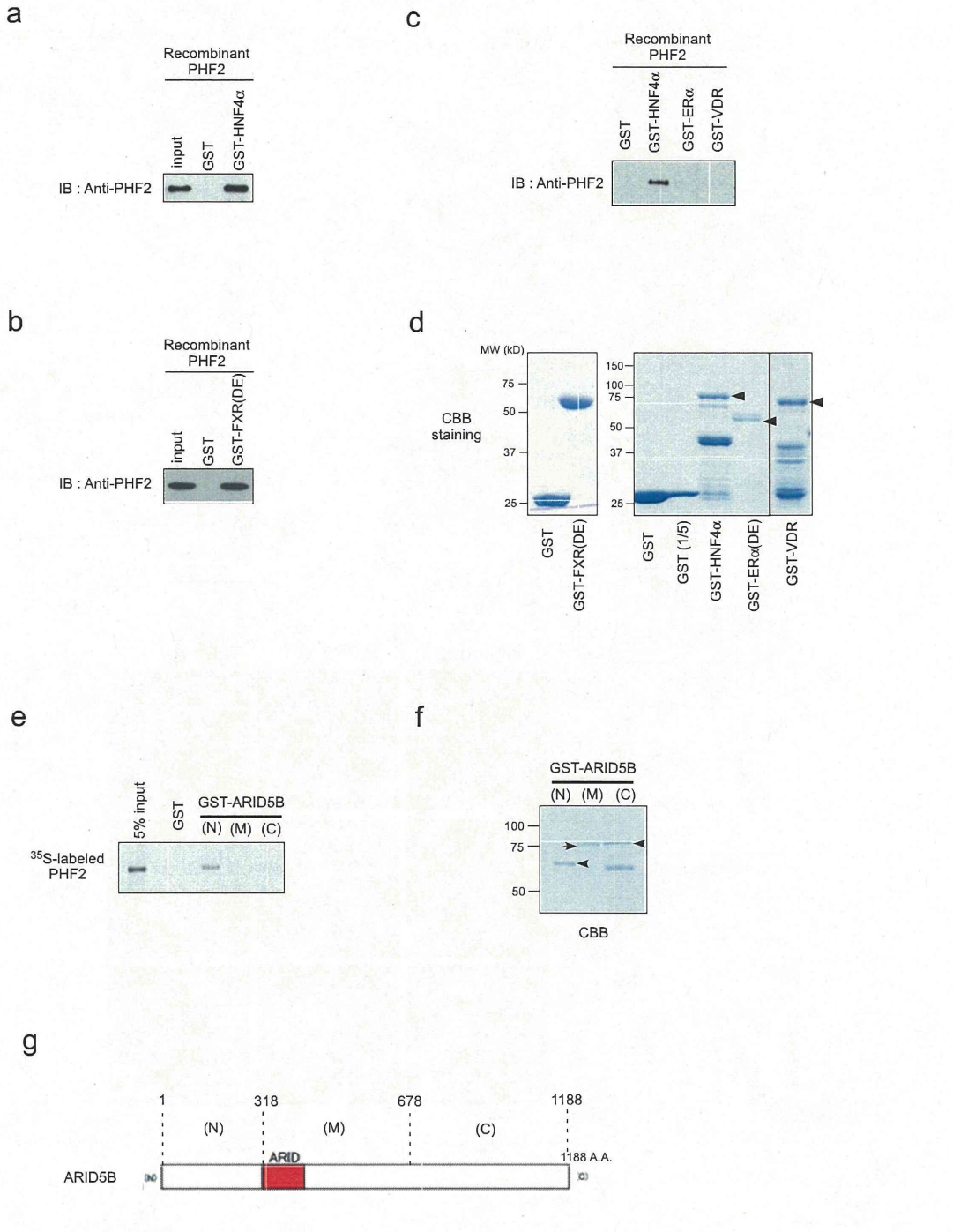

Figure S3 Direct association of PHF2/ARID5B with HNF4α and FXR. **a-d**, GST pull-down assay with recombinant PHF2 protein and GST-tagged FXR(DE), HNF4α, ERα (DEF), or VDR. Bound protein was detected with anti-PHF2 antibody. **e-g,** GST pull-down assay with ^{35}S-labeled PHF2 and GST-ARID5B mutants. GST-ARID5B mutants, described in (g), were incubated with *in vitro*-translated PHF2. Bound proteins were detected by autoradiography.

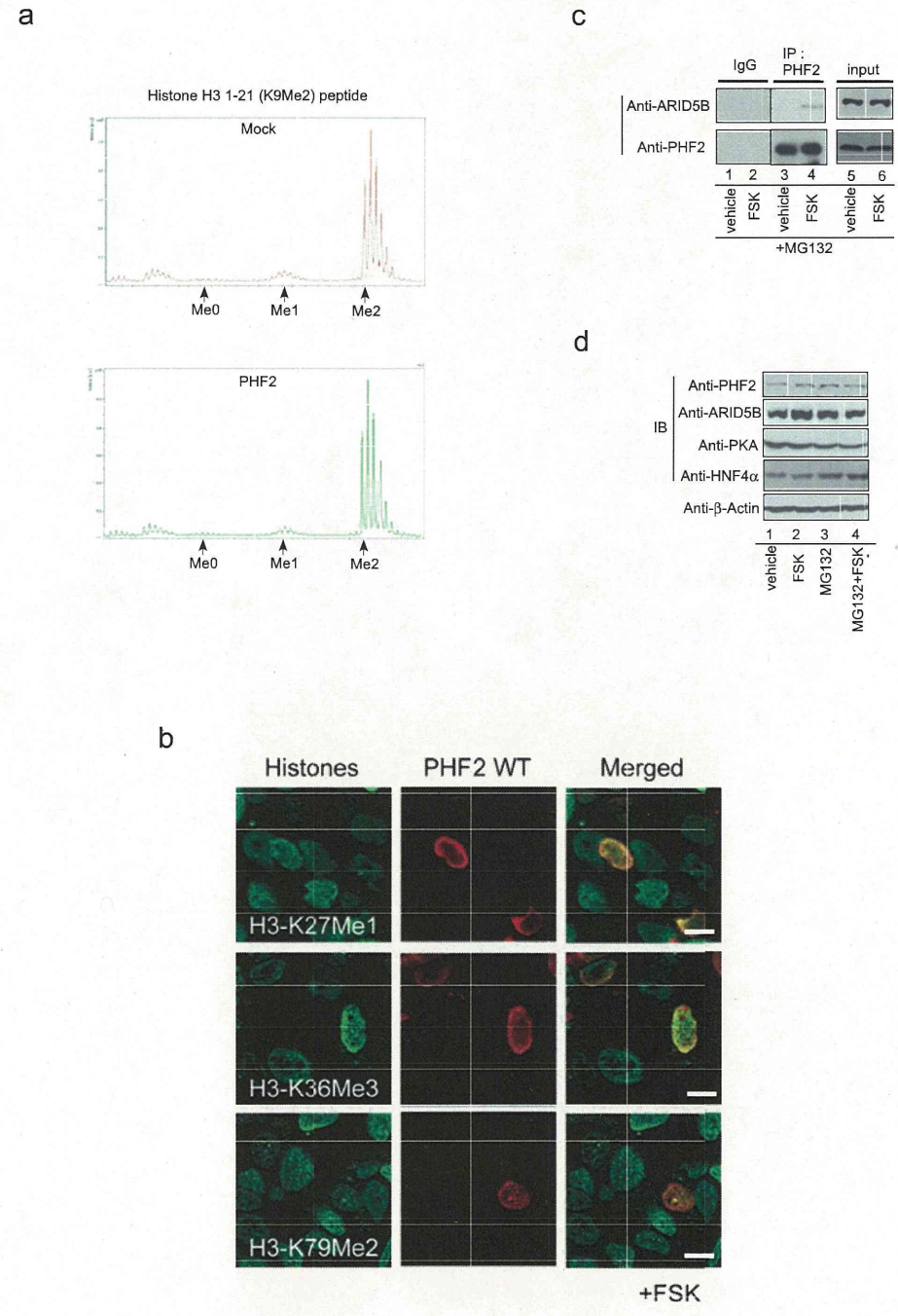

Figure S4 Demethylation activity of PHF2. **a,** Demethylase assay with H3 peptide. Purified PHF2 protein or mock immunoprecipitants incubated with PKA as in Fig. 3b was subjected to the demethylase assay with 0.2 μg of biotin-conjugated dimethyl histone H3 (Lys9) peptide (residues 1-21) (Upstate, 12-430). Demethylation was determined using MALDI-TOF/MS. Detailed methods were supplied as supplementary methods. **b,** Immunostaining of 293F cells was performed as described in Fig. 1f. **c,** Hepatocytes were treated with FSK (10^{-6} M) and MG132 (10^{-5} M) for two hrs. Total cell lysates were subjected to immunoprecipitation as indicated. **d,** FSK treatment did not alter protein expression levels of PHF2, ARID5B, or HNF-4α. Hepatocytes were treated with FSK (10^{-6} M) or MG132 (10^{-5} M) as indicated for 6 hrs. Cell lysates were subjected to Western blotting.

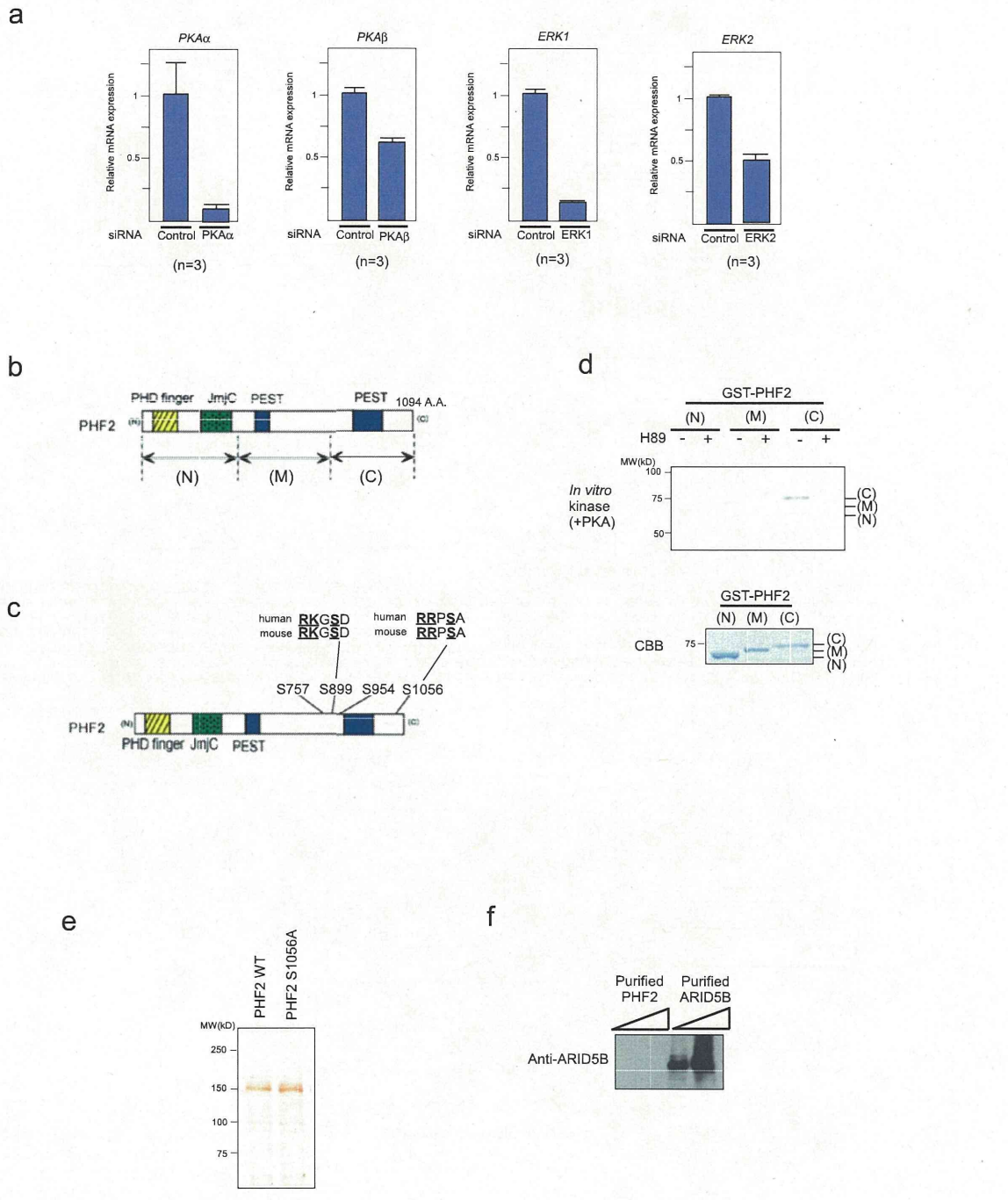

Figure S5 PKA phosphorylates PHF2 *in vitro* and *in vivo*. **a**, As controls for Fig. 2d, expression levels of the indicated genes were quantified by qPCR. Data shows average +/-S.D. (n=3). **b**, The schematic representation of deletion mutants of PHF2 used. **c**, The schematic representation of phosphorylation sites within PHF2 determined in Figure 2. **d**, PHF2 is phosphorylated by PKA at C-terminal region *in vitro*. *In vitro* kinase assay as indicated. **e**, 293F cells were transfected with FLAG-PHF2 or its mutant, and PHF2 was purified to of near homogeneity using anti-FLAG affinity column. Purified proteins were subjected to silver staining as indicated. **f**, Purified protein in Fig. 3a were subjected to Western blotting. Note that purified PHF2 did not include ARID5B.

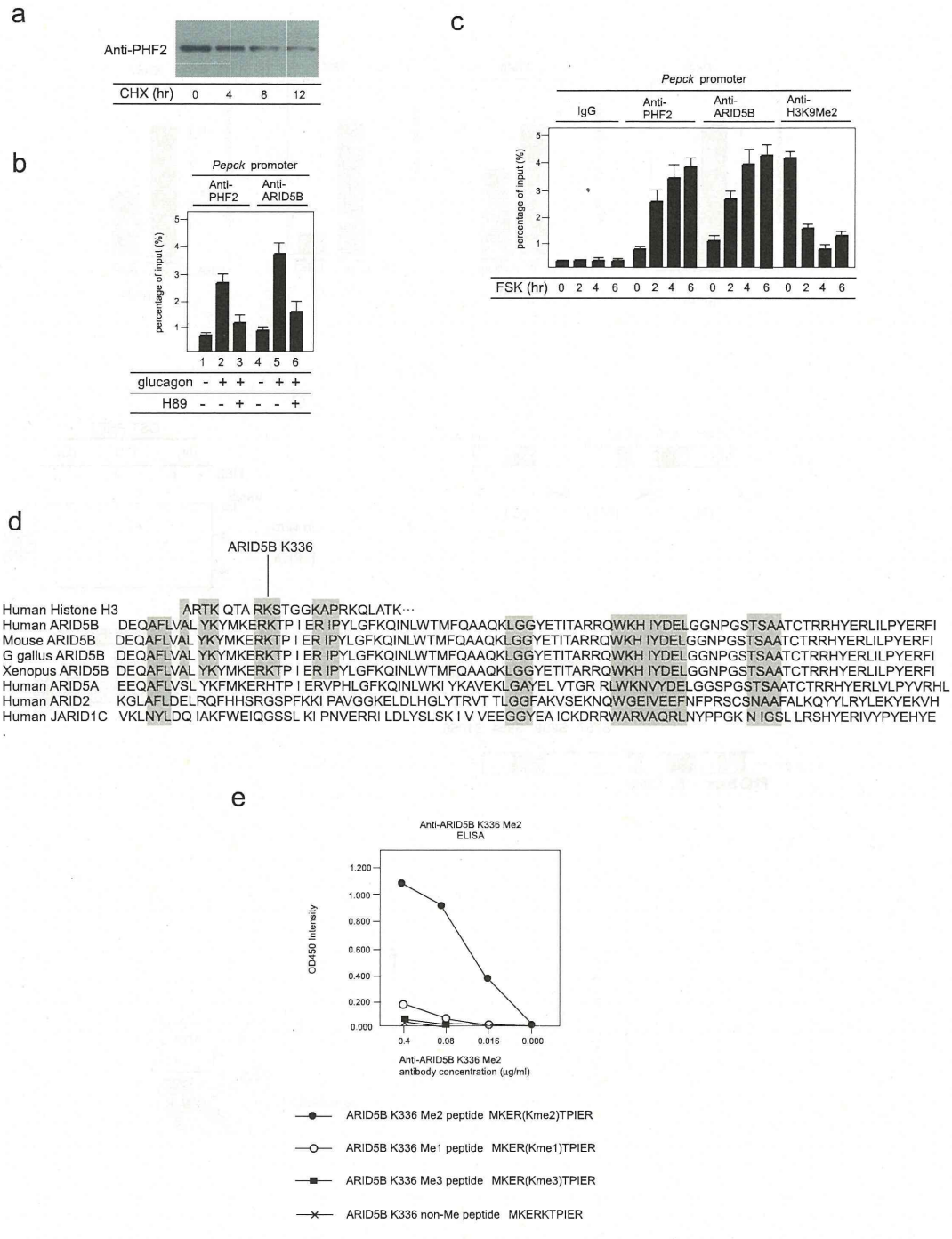

Figure S6 Promoter recruitment of PHF2/ARID5B. **a**, Protein turn-over of PHF2 as revealed by cycloheximide treatment. **b**, Recruitment of PHF2 and ARID5B to the *Pepck* promoter was abolished by a PKA inhibitor, H89. Hepatocytes were treated with glucagon and/or H89 (1 μM) for four hrs, then ChIP assay was performed using the indicated antibodies. **c**,, Co-recruitment of PHF2/ARID5B and demethylation of H3K9Me2 in *Pepck* promoter over similar time courses. Hepatocytes were treated with FSK for the indicated time, then a ChIP assay was performed as indicated. **d**, The schematic representation of amino acid sequences of ARID5B and other ARID family proteins. The sequence of histone H3K9 is also represented. **e**, Specificity of anti-ARID5B K336Me2 antibody. A rabbit polyclonal antibody against di-methylated Lys336 of ARID5B (anti-ARID5B K336Me2) was raised by using the di-methylated peptide [ARID5B K336Me2; MKER(Kme2)TPIER], and purified over a peptide-affinity column. The specificity of antibody toward K336Me2 peptide over non-methylated, mono-methylated, or tri-methylated peptides was determined by ELISA assays.